INL RPT-22-69180

DETAIL Component Scaling and Methodology Comparison

Dynamical System Scaling and Hierarchical Two-Tiered Scaling

September | 2022

Ramon Yoshiura
Computational Scientist, Integrated Energy & Market Analysis

Joshua Fischler
Irradiation Exp Thermal Hydraulics Analysis, Nuclear/Reactor Engineering

Aaron Epiney
Modeling/Simulation, Integrated Energy & Market Analysis

Zachary Ketrow
Graduate Student Intern, Oregon State University

IES
Integrated Energy Systems

INL is a U.S. Department of Energy National Laboratory operated by Battelle Energy Alliance, LLC

INL RPT-22-69180

DETAIL Component Scaling and Methodology Comparison

Dynamical System Scaling and Hierarchical Two-Tiered Scaling

Ramon Yoshiura
Computational Scientist, Integrated Energy & Market Analysis
Joshua Fischler
Irradiation Exp Thermal Hydraulics Analysis, Nuclear/Reactor Engineering
Aaron Epiney
Modeling/Simulation, Integrated Energy & Market Analysis
Zachary Ketrow
Graduate Student Intern, Oregon State University

September | 2022

Idaho National Laboratory
Integrated Energy Systems
Idaho Falls, Idaho 83415

http://www.ies.inl.gov

Prepared for the
U.S. Department of Energy
Office of Nuclear Energy
Under DOE Idaho Operations Office
Contract DE-AC07-05ID14517

Page intentionally left blank

SUMMARY

The purpose of this study was to develop a process to convert input signals from one facility into another by reflecting geometric and environmental settings. The Dynamic Energy Transport and Integration Laboratory (DETAIL) is a research facility in development. Its aim is to emulate the daily interactions among power production industry systems and receive real-time data from those systems as inputs. To convert signals and ensure that the temporal sequences and magnitudes reflect laboratory settings, the ability to scale and project data is essential. To demonstrate this ability, Dynamical System Scaling (DSS) and Hierarchical Two-Tiered Scaling (H2TS) (methodologies that enable systems to scale and project or extrapolate data sets to desired environments while conserving the observed behavior based on first principles) were applied to DETAIL's thermocline thermal storage system in the Thermal Energy Distribution System (TEDS) facility and solid-oxide electrolysis cell in the High Temperature Hydrogen Electrolysis (HTHE) facility. Both thermocline and electrolysis cell systems were successfully scaled, and test cases were conducted to generate a doubly accelerated energy charge and discharge in reference to past experimental data from the facilities. The research results represented a case for the thermocline system that required signals to be accelerated without altering the stored energy. To enhance the quality of the accelerated data, error propagation analyses were conducted on DSS post-processing terms to determine the consequences of raw-data-associated errors.

Page intentionally left blank

CONTENTS

FIGURES

TABLES

Page intentionally left blank

ACRONYMS

IES	Integrated Energy System
DETAIL	Dynamic Energy Transport and Integration Laboratory
DSS	Dynamical System Scaling
H2TS	Hierarchical Two-Tiered Scaling
CMT	Core Makeup Tank
TTSS	Thermocline Thermal Storage System
TEDS	Thermal Energy Distribution System
SOEC	Solid-Oxide Electrolysis Cell
HTHE	High Temperature Hydrogen Electrolysis
INL	Idaho National Laboratory
NPP	Nuclear Power Plant
PIRT	Phenomena Identification and Ranking Table
HX	Heat Exchanger
V&V	Validation and Verification
MAGNET	Microreactor Agile Non-Nuclear Experimental Testbed
MARVEL	Microreactor Applications Research Validation and Evaluation
UQ	Uncertainty Quantification

Page intentionally left blank

DETAIL Component Scaling and Methodology Comparison

1. INTRODUCTION AND BACKGROUND

Integrated energy systems (IESs) are crucial components for maximizing the efficiency of energy usage and complying with growing power demands [1]. The current state of power supply is a superposition of all available power production methodologies, including fossil fuel, nuclear, solar, wind, and others [2]. The coordination of these components is essential to avoid instances of energy waste and outage during emergencies. Recent representative examples of outages and imbalances in grid load were observed in Texas in 2021, when record-breaking low temperatures simultaneously impacted energy production and increased power demand [3], and in Argentina in 2022, when prolonged unexpectedly high temperatures decreased power production efficiency, increased power demand, and eventually affected the supply of quality water as purification systems could not be operated at full capacity [4]. Some of the typical mitigations of these events include temporarily limiting energy usage, importing electricity from neighboring grid operators, utilizing stored energy, or load shedding [5]. The role of IESs is to dynamically respond to parameters such as power demand, grid frequency, and grid load balance. At a given time of day, as power usage and power production (especially for renewable energy sources) fluctuate, IESs not only have the potential to regulate power production distribution based on each individual power utility but can also automatically turn on energy storing mechanisms (hydrogen production, thermal storage, etc.) for times of unavoidable cases of excess energy, thereby preventing grid frequency increase [5].

The IES that is represented in the Dynamic Energy Transport and Integration Laboratory (DETAIL) is a combination of thermal storage, battery testing, hydrogen production, electrical vehicle charging, a digital real-time power grid, distributed energy and microgrid, power plant operation, and a non-nuclear microreactor experimental testbed [6]. The goal is to have each system communicate and emulate an IES environment. This includes receiving external signals from industry utilities as inputs to enable real-time data-driven experiments. One component to consider is the design of the experiments when one DETAIL system is interacting with another. Since each facility in DETAIL is operated by individual specialized group, the physical ties between the systems are uncharted boundaries and for every new experiment design, the integral effects on all systems must be evaluated. Another component to consider is how to translate the industry data into lab configurations. Lab-scale facilities are downscaled versions of industry-scale power plants or energy processing utilities and inputting raw data would not realistically match lab configurations. For this purpose, a data post-processing step is required to convert output data into configurable input data in the correct sequence, based on physics (i.e., when industry-scale data comprise data points for every hour, each data point needs to be converted to correspond to a lab-scale data point).

The purpose of this research was to implement Dynamical System Scaling (DSS) and Hierarchical Two-Tiered Scaling (H2TS) to project, extrapolate or derive initial and boundary conditions, data sets, and new tests based on existing knowledge and generated data from each target application for the facility in question. The DSS (time-dependent) and H2TS (static) scaling procedures allow variations in system parameters that are defined by design objectives, the detection of transient distortions, and unique illustrations of generated data [7]. Out of the numerous capabilities provided by DSS and H2TS, the data synthesis and scaling analysis tools are of particular interest. The utilization of both tools grants users the ability to analyze critical data, and the mathematical algorithms to perform such activities are codable.

One example of using DSS and H2TS scaling analysis tools to engineer components is the parametric study of the core makeup tank (CMT) from Westinghouse AP1000, which was simulated via RELAP5 [8]. Work in the last fiscal year developed DSS code in RAVEN, and CMT was downscaled identically to work described in Li et al. [8] in size while maintaining the same draining time [9]. Another example using DSS is the downscaling of the Experimental Breeder Reactor-II metallic fuel rods to shorten the required irradiation time [10]. Based on neutronics, reactor physics, and thermohydraulics, the fuel rod geometry for the desired irradiation time was determined. The application of DSS and other modern scaling techniques to systems and models that are developed under the IES program constitutes a logical continuation of previous IES work, in which systems were analyzed using traditional scaling approaches [11].

To apply the test extrapolation case, our research team selected a thermocline thermal storage system (TTSS) in the Thermal Energy Distribution System (TEDS) facility and the solid-oxide electric cell (SOEC) in the High Temperature Hydrogen Electrolysis (HTHE) facility at Idaho National Laboratory (INL), which is part of DETAIL under the IES program. One of the missions of the IES program is to optimize thermodynamic and financial efficiency through system integration [12]. The TEDS and HTHE facility were designed to demonstrate thermal system functions for the generation, storage, delivery, and use of high-quality energy products to support industrial processes and grid infrastructure [13]. Together, TEDS and HTHE represents the required communication between heat storage and heat utilization.

Currently, the validation activities for the TEDS and HTHE models are being conducted in Dymola (Modelica-based) with collected facility data [14]. The simulation covers transient physics-based models for scaled-up IESs, including nuclear power plant (NPP) designs from Westinghouse and NuScale Power. Coupling reactor modules with heat transfer loops to test the feasibility of heat extraction from NPPs requires the simulation of the systems' performances in advance. The simulation must be capable of reproducing experimental results. Therefore, a set of representative experiments need to be defined and used to validate the models against experimental results. For validation cases, such as that of TEDS, the current research focuses on projecting data and the required operational conditions to accelerate the core phenomena as a potential future test design that could support code validation.

2. DYNAMICAL SYSTEM SCALING THEORY

The DSS approach to system scaling is based on transforming the typical view of a process into a special coordinated system in terms of the parameter of interest and its agents of change [15]. By parameterizing a process using a time term, which is introduced later in this section, the reproduced data can be converted into the special three-coordinate system (also called the phase space) and form a geometry with curves along the surface that contain invariant and intrinsic properties. The remainder of this section is a review of DSS theory, which was introduced into publications by Reyes [[7],[15],[16]] and was used in this analysis for the thermocline scaling. The parameter of interest is defined as a conserved quantity within a control volume:

$$\beta(t) = \frac{1}{\Psi_0} \iiint_V \psi(\vec{x}, t)\, dV \tag{1}$$

Where β is defined as the volume integral of the time- and space-dependent conserved quantity ψ when normalized by a time-independent value Ψ_O, which characterizes the process. The agents of change are defined as the first derivative of the normalized parameter of interest:

$$\omega = \frac{1}{\Psi_0}\frac{d}{dt} \iiint_V \psi(\vec{x}, t)\, dV = \iiint_V \left(\phi_v + \phi_f\right) dV + \iint_A (\vec{J} \cdot \vec{n})\, dA - \iint_A \psi(\vec{v} - \vec{v}_s) \cdot \vec{n}\, dA \tag{2}$$

The changes are categorized into three components: volumetric, surface, and quantity transport. The agents of change are also the sum of the individual agents of change:

$$\omega(t) = \frac{1}{\Psi_0}\frac{d}{dt} \iiint_V \psi(\vec{x}, t) = \sum_{i=1}^{n} \omega_i \tag{3}$$

The relationship between ω and β is the following:

$$\omega(t) = \frac{d\beta}{dt}\Big|_t = \sum_{i=1}^{n} \omega_i \tag{4}$$

where ω is the first derivative of the reference time. As defined in Einstein and Infeld, time is a value that moves in constant increments [17]. The process-dependent term in DSS is called process time:

$$\tau(t) = \frac{\beta(t)}{\omega(t)} \tag{5}$$

Using β, ω, and τ, the transient of the parameter of interest is characterized as geometric data using the coordinate system shown in Figure 1. To measure the progression difference between the reference time and process time in terms of the reference time, the idea of temporal displacement rate (D) is adopted:

$$D(t) = \frac{d\tau - dt}{dt} = -\frac{\beta}{\omega^2}\frac{d\omega}{dt} \tag{6}$$

The interval of the process time is:

$$d\tau = \tau_S = \int (1 + D)\, dt \tag{7}$$

Applying the process action to normalize the phase space coordinates produces the following normalized terms:

$$\widetilde{\Omega} = \omega\tau_S,\ \tilde{\beta} = \beta,\ \tilde{t} = \frac{t}{\tau_S},\ \widetilde{D} = D \tag{8}$$

The normalized agents of change $(\widetilde{\Omega})$ is also referred as the effect parameter, and is used with the parameter of interest to visualize the phase space of the transient. A representation of the phase-space diagram is provided in Figure 2.

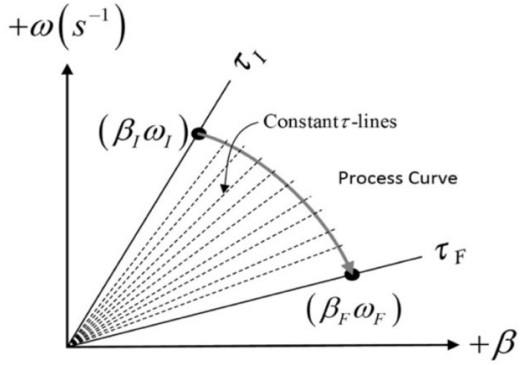

Figure 1. The β-ω-τ coordinate system with the representation of data evolution defined with changing process time where subscript "*I*" is the initial state and "*F*" is the final state [7].

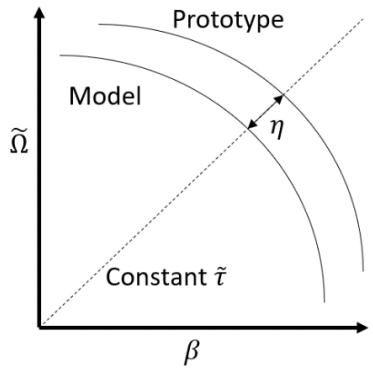

Figure 2. Phase space defined by the effect parameter ($\tilde{\Omega}$) and parameter of interest (β). η is the geodesic distance between model and prototype data points along constant normalized process time.

To demonstrate a simple example, suppose the parameter of interest is an arbitrary sine function. The agents of change and its first derivative are then:

$$\beta = \sin(ct) \rightarrow \omega = c\cos(ct) \rightarrow \frac{d\omega}{dt} = -c^2\sin(ct) \tag{9}$$

The temporal displacement is:

$$D = -\frac{\beta}{\omega^2}\frac{d\omega}{dt} = c\tan^2(ct) \tag{10}$$

The process action for reference time interval of (t_I, t_F) is: (11)

$$\tau_S = \int(1+D)\,dt = (\tan(ct) - \tan^{-1}(\tan(ct)))\big|_{t_I}^{t_F} \tag{12}$$

The process action normalized terms are:

$$\tilde{\Omega} = \omega\tau_S = c\cos(ct)\left[(\tan(ct) - \tan^{-1}(\tan(ct)))\big|_{t_I}^{t_F}\right],\ \tilde{t} = \frac{t}{(\tan(ct) - \tan^{-1}(\tan(ct)))\big|_{t_I}^{t_F}} \tag{13}$$

Although the provided example is given as an explicit equation, for realistic cases, the transient parameter of interest (β) values is typically in data array form. To determine the agents of change (ω) and temporal displacement rate (D), discrete numerical methods for derivatives and integrals are required for total DSS analysis.

The scaling relationship between the prototype and model can be defined for both β and ω and represents the scaling of the parameter of interest and its corresponding agents of change (or the frequency obtained from the units of time):

$$\lambda_A = \frac{\beta_M}{\beta_P},\ \lambda_B = \frac{\omega_M}{\omega_P} \tag{14}$$

Where the subscripts M and P stand for the model and prototype, respectively. The application of these scaling ratios to Equations (5), (6), and (8) provides the scaling ratios for other parameters as well:

$$\frac{t_M}{t_P} = \frac{\lambda_A}{\lambda_B},\ \frac{\tau_M}{\tau_P} = \frac{\tau_{S,M}}{\tau_{S,P}} = \frac{\lambda_A}{\lambda_B},\ \frac{\tilde{\beta}_M}{\tilde{\beta}_P} = \lambda_A,\ \frac{\tilde{\Omega}_M}{\tilde{\Omega}_P} = \lambda_A,\ \frac{\tilde{\tau}_M}{\tilde{\tau}_P} = 1,\ \frac{D_M}{D_P} = 1 \tag{15}$$

The normalized agent of change is the sum in the same respect:

$$\tilde{\Omega} = \sum_{i=1}^{k}\tilde{\Omega}_i \tag{16}$$

The ratio of Ω is expressed in the following alternative form:

$$\widetilde{\Omega} = \frac{\widetilde{\Omega}_M}{\widetilde{\Omega}_P} = \frac{\sum_{i=1}^{k} \widetilde{\Omega}_{M,i}}{\sum_{i=1}^{k} \widetilde{\Omega}_{P,i}} = \frac{\widetilde{\Omega}_{M,1}+\widetilde{\Omega}_{M,2}+\cdots+\widetilde{\Omega}_{M,k}}{\widetilde{\Omega}_{P,1}+\widetilde{\Omega}_{P,2}+\cdots+\widetilde{\Omega}_{P,k}} \tag{17}$$

By the law of scaling ratios, the following must be true:

$$\lambda_A = \frac{\widetilde{\Omega}_{M,1}}{\widetilde{\Omega}_{P,1}} = \frac{\widetilde{\Omega}_{M,2}}{\widetilde{\Omega}_{P,2}} = \cdots = \frac{\widetilde{\Omega}_{M,k}}{\Omega_{P,k}} \tag{18}$$

From Reyes, the scaling methods and similarity criteria are subdivided into five categories: 2-2 affine, dilation, β-strain, ω-strain, and identity [15]. Table 1 summarizes the similarity criteria. Despite the five categories, in essence, all are 2-2 affine, with the exception of the partial scaling ratio values being 1.

Table 1. Scaling methods and similarity criteria that result from two-parameter transformations [15]

Basis for Process Space-Time Coordinate Scaling				
Metric Invariance	$d\tilde{\tau}_P = d\tilde{\tau}_M$	and	Covariance Principle	$\frac{1}{\omega_P}\frac{d\beta_P}{dt_P} = \frac{1}{\omega_M}\frac{d\beta_M}{dt_M}$
$\beta - \omega$ Coordinate Transformations				
2-2 Affine	Dilation	β-Strain	ω-Strain	Identity
$\beta_R = \lambda_A$	$\beta_R = \lambda$	$\beta_R = \lambda_A$	$\beta_R = 1$	$\beta_R = 1$
$\omega_R = \lambda_B$	$\omega_R = \lambda$	$\omega_R = 1$	$\omega_R = \lambda_B$	$\omega_R = 1$
Similarity Criteria				
$\widetilde{\Omega}_R = \lambda_A$	$\widetilde{\Omega}_R = \lambda$	$\widetilde{\Omega}_R = \lambda_A$	$\widetilde{\Omega}_R = 1$	$\widetilde{\Omega}_R = 1$
$\tau_R = t_R = \frac{\lambda_A}{\lambda_B}$	$\tau_R = t_R = 1$	$\tau_R = t_R = \lambda_A$	$\tau_R = t_R = \frac{1}{\lambda_B}$	$\tau_R = t_R = 1$

The selection process is completely dependent on the system to be scaled and the restrictions applied. According to personal experience, limitations such as geometry, material properties, and manufacturing methods are major components that constrain the available types capable of scaling while abiding to research objectives.

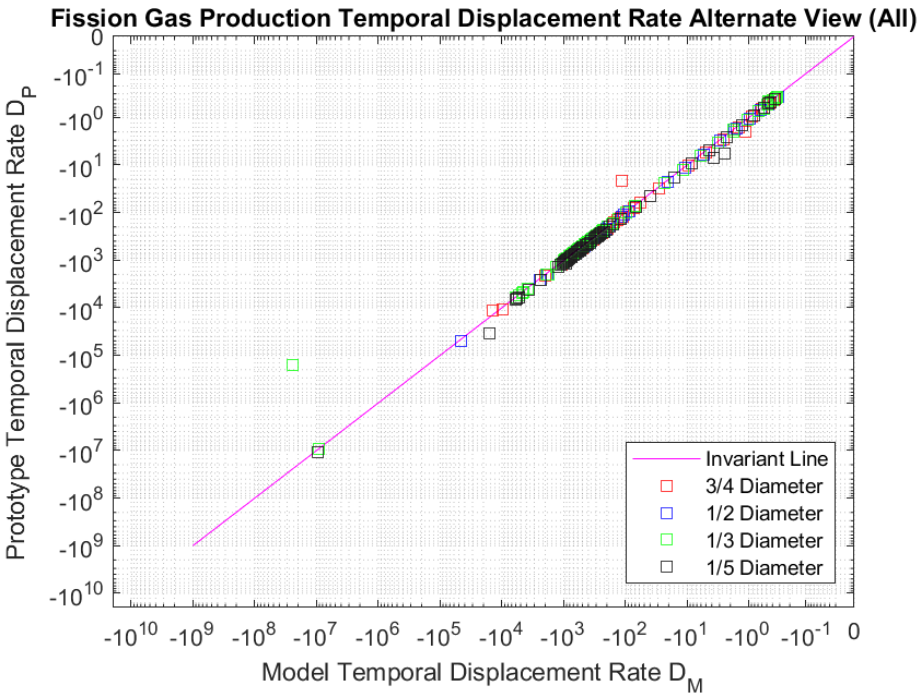

Figure 3. The prototype and model temporal displacement rate as axes added with the ideal 45-degree line for fission gas production simulated in BISON. If model and prototype values are perfectly scaled, each corresponding data point should overlap with the ideal line *[10]*.

3. HIERARCHICAL TWO-TIERED SCALING THEORY

The H2TS consists of four fundamental domains: subdivision of interacting systems, identification of scaling level, system scaling analysis, and process system scaling analysis [7]. The subdivision and scaling identification is accomplished by conducting a Phenomena Identification and Ranking Table (PIRT) activity to discern the existing subsystems, modules, constituents, and phases. Depending on the weighting of each component and developed equations, the scaling emphasis on either system scaling analysis (also called top-down scaling) or process scaling analysis (also called bottom-up scaling) may differ from one project to another. In some cases, a top-down scaling reveals important processes that may be need to be addressed in the bottom-up scaling.

To express each H2TS task while abiding to DSS's conserved quantity within a control volume equation format, Equation (2) will be used as the main starting point for describing H2TS terminologies. Equation (2) is modified to Equation (14):

$$\frac{dV_l\psi_l}{dt} = S_l + \sum_{x=1}^{m} j_{l,x}A_{l,x} + \sum_{x=1}^{m} \psi_{l,x}\left(v_{l,x} - v_{s,l,x}\right)A_{l,x} \tag{19}$$

Where volumetric, surface, and quantity transport are provided for each constituent l. V_l is the control volume, ψ_l is the conserved quantity per volume, S_l is the volumetric source or sink, j_l is the quantity flux, A_l is the sectional area, v_l is the fluid velocity, and $v_{s,l}$ control volume surface velocity. For simplicity, the fluid velocity difference will be expressed as Δv. Terms holding units are replaced with the following dimensionless form:

$$V_l^+ = \frac{V_l}{V_{l,0}},\ \psi^+ = \frac{\psi_l}{\psi_{l,0}},\ S_l^+ = \frac{S_l}{S_{l,0}},\ j_{l,x}^+ = \frac{j_{l,x}}{j_{l,x,0}},\ A_{l,x}^+ = \frac{A_{l,x}}{A_{l,x,0}},\ \psi_{l,x}^+ = \frac{\psi_{l,x}}{\psi_{l,x,0}},\ \Delta v_{l,x}^+ = \frac{\Delta v_{l,x}}{\Delta v_{l,x,0}} \tag{20}$$

Replacing terms in Equation (19) into Equation (18) provide the dimensionless form:

$$V_{l,0}\psi_{l,0}\frac{dV_l^+\psi_l^+}{dt} = S_{l,0}S_l^+ + \sum_{x=1}^{m} j_{l,x,0}A_{l,x,0}j_{l,x}^+A_{l,x}^+ + \sum_{x=1}^{m}\psi_{l,x}\Delta v_{l,x,0}A_{l,x,0}\psi_{l,x}^+\Delta v_{l,x}^+A_{l,x}^+ \quad (21)$$

The first task in H2TS is to derive the residence time. This specialized temporal quantity is used to determine how long a certain system or process transient prevails. For steady state analysis, the residence time is still used to determine system similarity or calculate the full-time duration of the scaled phenomenon of interest:

$$\text{Residence Time: } \tau_{RS} = \frac{V_{l,0}\psi_{l,0}}{S_{l,0}} \quad (22)$$

In this case, the residence time is defined to be division between the reference conserved quantity and reference source or sink. The unit is the inverse of the per time quantity. To extract meaningful information that is utilized to determine the components affecting the conversed quantity, the characteristic time ratio for each component of change is derived in dimensionless form and describes the relative evolution of the component transient. Considering the residence time equation, the characteristic time ratios can be determined from Equation (20):

$$\tau_{RS}\frac{dV_l^+\psi_l^+}{dt} = S_l^+ + \sum_{x=1}^{m}\frac{j_{l,x,0}A_{l,x,0}}{S_{l,0}}j_{l,x}^+A_{l,x}^+ + \sum_{x=1}^{m}\frac{\psi_{l,x,0}\Delta v_{l,x,0}A_{l,x,0}}{S_{l,0}}\psi_{l,x}^+\Delta v_{l,x}^+A_{l,x}^+ \quad (23)$$

Each component coefficient about reference values is dimensionless and can be shown as the following:

$$\Pi_1 = \frac{j_{l,x,0}A_{l,x,0}}{S_{l,0}},\ \Pi_2 = \frac{\psi_{l,x,0}\Delta v_{l,x,0}A_{l,x,0}}{S_{l,0}} \quad (24)$$

In full form, Equation (22) is represented as:

$$\tau_{RS}\frac{dV_l^+\psi_l^+}{dt} = S_l^+ + \sum_{x=1}^{m}\Pi_1 j_{l,x}^+A_{l,x}^+ + \sum_{x=1}^{m}\Pi_2\psi_{l,x}^+\Delta v_{l,x}^+A_{l,x}^+ \quad (25)$$

Depending on the quantity of each characteristic time ratio, the following are behaviors determined by the reference value combinations: (1) if smaller than 1, only a small amount of the conserved quantity is transported relative to the generated or destroyed amount, and (2) if equal to 1 or larger, relatively significant amounts of the conserved quantity are transported. If the denominator of characteristic time ratios Π_1 and Π_2 included $\psi_{l,0}$, then relative target is the conserved quantity reference value. Decisions upon selecting which combinations to derive residence time and characteristic time ratio can affect how users interpret the relations of conserved quantity and its components of change.

The scaling aspect of H2TS is to determine the model system geometry and environment conditions based on system similarity. This includes matching characteristic time ratio values that have been identified in the PIRT process.

$$\Pi_P = \Pi_M \quad (26)$$

An example can be shown for the quantity flux characteristic time ratio by considering the protype and model reference values:

$$\Pi_P = \left.\frac{j_{l,x,0}A_{l,x,0}}{S_{l,0}}\right|_P = \left.\frac{j_{l,x,0}A_{l,x,0}}{S_{l,0}}\right|_M = \Pi_M \quad (27)$$

Depending on the reference value flexibility, some parameters are possibly unchangeable and may restrict the model design. In the case where model quantity flux is forced to be equal to prototype values and the model conserved quantity generation or the sink is half, the reference surface area must be half as well:

$$j_{l,x,0}\big|_M = j_{l,x,0}\big|_P, S_{l,0}\big|_M = \frac{S_{l,0}\big|_P}{2} \rightarrow A_{l,x,0}\big|_M = \frac{A_{l,x,0}\big|_P}{2} \tag{28}$$

Although it would be ideal to match all characteristic time ratios, it is said to be impossible, and negligence of discarded terms are sources of scaling distortion [7].

4. THERMAL ENERGY DISTRIBUTION SYSTEM SCALING ANALYSIS

The TEDS TTSS system was selected as the first demonstration case from which to extrapolate data. The TEDS facility is one of the energy storage systems in DETAIL, which specializes in thermal charge, storage, and discharge. It comprises the following seven components: (1) a therminol tank, (2) an oil–glycol heat exchanger (HX), (3) a filtration system, (4) a driving pump, (5) a heat injection system, (6) a TTSS, and (7) a therminol regulation system. The TTSS sits between the hot and cold lines that allow flows from either section, depending on the operation mode [12] and is shown in Figure 4:

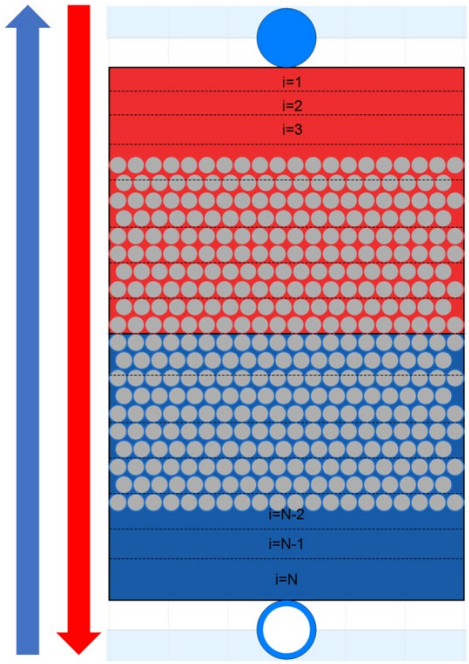

Figure 4. TTSS nodal representation and charge modes.

The following sections characterize the conservation rules and non-dimensionalize the process when necessary.

4.1 Thermal Energy Distribution System Governing Equations

Based on the publication of Konor et al. [12], the following governing equations were used and modified for the purpose of scaling in DSS and H2TS methodologies:

4.1.1 Mass Flow Rate

When the mass flow rate from the inlet is m, then by conservation of mass, the mass flow rate within the TTSS must be equivalent:

$$\dot{m} = \rho_{in} v_{z,in} \pi R_{in}^2 = \rho_{th} v_{z,th} \varepsilon \pi R_{th}^2 \tag{29}$$

Where ρ_{in} is the inlet density, ρ_{th} is the TTSS density, $v_{z,in}$ is the inlet axial velocity, $v_{z,th}$ is the TTSS axial velocity, R_{in} is the inlet pipe radius, ε is the porosity (ratio of fluid to filler), and R_{th} is the TTSS fluid tank radius. The TTSS axial velocity is the following:

$$v_{z,th} = \frac{\rho_{in} R_{in}^2 v_{z,in}}{\rho_{th} \varepsilon R_{th}^2} \tag{30}$$

4.1.2 Conservation of Mass

In cylindrical coordinates, the compressible conservation of mass is:

$$\frac{\partial \rho_{th}}{\partial t} + \frac{1}{r}\frac{\partial (\rho_{th} r v_{r,th})}{\partial r} + \frac{v_{\theta,th}}{r}\frac{\partial (\rho_{th} v_{\theta,th})}{\partial \theta} + \frac{\partial v_{z,th}}{\partial z} = 0 \tag{31}$$

Where $v_{r,th}$ is the TTSS radial velocity and $v_{\theta,th}$ is the TTSS azimuthal velocity. By expanding the terms and ignoring the radial and azimuthal velocities, the differential density is:

$$\frac{\partial \rho_{th}}{\partial t} = -v_z \frac{\partial \rho_{th}}{\partial z} - \rho_{th} \frac{\partial v_z}{\partial z} \tag{32}$$

4.1.3 Conservation of Momentum

In cylindrical coordinates, the compressible conservation of momentum in the axial direction is:

$$\frac{D(\rho_{th} v_{z,th})}{Dt} = -\frac{\partial P}{\partial z} + \mu_{th}\left(\frac{1}{r}\frac{\partial v_{z,th}}{\partial r} + \frac{\partial^2 v_{z,th}}{\partial r^2} + \frac{\partial^2 v_{z,th}}{\partial z^2}\right) \tag{33}$$

Where P is the TTSS internal pressure. By expanding the terms, the differential axial velocity is:

$$\frac{\partial v_{z,th}}{\partial t} = -\frac{v_{z,th}}{\rho_{th}}\frac{\partial \rho_{th}}{\partial t} - \frac{1}{\rho_{th}}\frac{\partial P}{\partial z} + \nu\left(\frac{1}{r}\frac{\partial v_{z,th}}{\partial r} + \frac{\partial^2 v_{z,th}}{\partial r^2} + \frac{\partial^2 v_{z,th}}{\partial z^2}\right) \tag{34}$$

4.1.4 Conservation of Energy

From Konor et al. [11], the thermocline heat transfer equation that characterizes the energy conservation of a fluid flow through porous media for low- and no-flows is (originally from Gunn 1978 [18] and modified in [19]):

$$\rho_{th} c_{P,th} \varepsilon \pi R_{th}^2 dz \frac{\partial T_{th}}{\partial t} = \rho_{th} \varepsilon \pi R_{th}^2 v_{z,th}(h_z - h_{z+dz}) + h_c S_r\left(T_{fr} - T_{th}\right)dz + \dot{Q}_{losses} \tag{35}$$

Where ε is the porosity, h_z is the specific enthalpy of the current node, h_{z+dz} is the specific enthalpy of the next axial node, h_c is the convective heat transfer coefficient between the fluid and filler, S_{fr} is the filler temperature, T_{th} is the TTSS fluid temperature, dz is the axial distance between each node, and $\dot{Q}_{losses}$ is the heat conduction through the walls. When the specific enthalpy is replaced by the specific heat and temperature at the node, the heat transfer equation is:

$$\rho_{th}c_{P,th}\varepsilon\pi R_{th}^2 dz\frac{\partial T_{th}}{\partial t} = \rho_{th}\varepsilon\pi R_{th}^2 v_{z,th}\left(c_{P,z,th}T_{th,z} - c_{P,z+dz,th}T_{th,z+dz}\right) \quad (36)$$
$$+h_c S_r\left(T_{fr} - T_{th}\right)dz + \dot{Q}_{losses}$$

By dividing both sides by dz and considering the specific enthalpy difference portion as a form of first-order forward numeric differentiation, the difference can be rewritten as the spatial first derivative of the specific enthalpy in the axial direction:

$$\rho_{th}c_{P,th}\varepsilon\pi R_{th}^2 dz\frac{\partial T_{th}}{\partial t} = \rho_{th}\varepsilon\pi R_{th}^2 v_{z,th}\frac{\partial\left(c_{P,th}T_{th}\right)}{dz} + h_c S_r\left(T_{fr} - T_{th}\right) + \frac{\dot{Q}_{losses}}{dz} \quad (37)$$

By using Equation (28) for the TTSS axial velocity and expanding the terms, it can be reorganized as:

$$\frac{\partial T_{th}}{\partial t} = \frac{\rho_{in}R_{in}^2 v_{z,in}}{\rho_{th}c_{P,th}R_{th}^2}\left(T_{th}\frac{\partial c_{P,th}}{\partial z} + c_{P,th}\frac{\partial T_{th}}{\partial z}\right) + \frac{h_c S_r\left(T_{fr}-T_{th}\right)}{\rho_{th}c_{p,th}\varepsilon\pi R_{th}^2} + \frac{\pi R_w^2}{\rho_{th}c_{p,th}\varepsilon\pi R_{th}^2}\left(\frac{k}{r}\frac{\partial T_w}{\partial r} + \frac{\partial k}{\partial r}\frac{\partial T_w}{\partial r} + k\frac{\partial^2 T_w}{\partial r^2}\right) \quad (38)$$

Where T_w is the wall temperature.

4.2 Thermal Energy Distribution System Dynamical System Scaling

The TEDS TTSS DSS scaling has been published under [20] to satisfy previous milestones. The content shown in this report will be a summary of the publication only providing end results.

4.2.1 Scaling Objective

As a test case for data projection, the transient data set of the double accelerated heat charge and discharge while conserving the amount of heat storage was determined without altering system geometry based on past data. The conducted research determined the following steps to complete the data projection: (1) discretize axially and radially some of the differential equations to include data points at specific measurement locations, (2) non-dimensionalize parameters of interest, (3) determine scaling ratios by considering law of scaling ratio, (4) commence coordinate transformations selection process, and (5) determine projected data based on assumptions, adaptions, and facility restrictions.

4.2.2 Scaling Results and Conclusions

Considering the available data and discretized form of Equation (36), the following parameters were non-dimensionalized: (1) thermocline centerline middle fluid temperature (T_{th} at i),(2) inlet fluid temperature (T_{in} at $i - n/2$), (3) outlet temperature (T_{out} at $i + n/2$), (4) wall temperature (T_w at i, j), (5) ambient temperature (T_{amb} at $i, j + 2$), and (6) inlet velocity ($v_{z,in}$ at $i - n/2$ when charging and at $i + n/2$ when discharging). Unfortunately, due to the limitations of measurement equipment, terms such as thermocline filler temperature and velocity cannot be collected. Figure 5 shows the locations of existing data used for the DSS scaling and Equation (38) is the relevant defined scaling ratios.

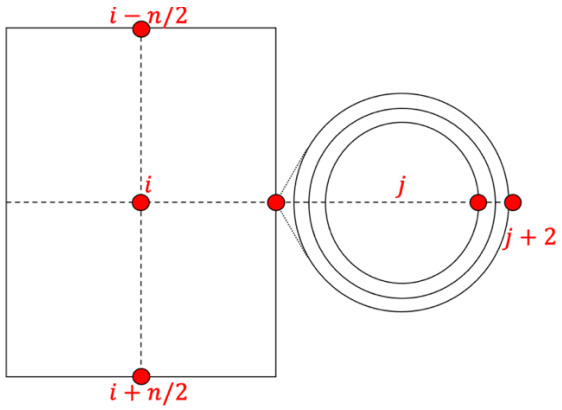

Figure 5. Nodal locations of each data measurement.

Thermocline Height:

$$\lambda_{A,z} = \frac{z_M^+}{z_P^+}, \quad \lambda_{B,z} = \frac{\left.\frac{\partial z^+}{\partial t}\right|_M}{\left.\frac{\partial z^+}{\partial t}\right|_P}$$

Thermocline Radius:

$$\lambda_{A,r} = \frac{r_M^+}{r_P^+}, \quad \lambda_{B,r} = \frac{\left.\frac{\partial z^+}{\partial t}\right|_M}{\left.\frac{\partial z^+}{\partial t}\right|_P}$$

Thermocline Centerline Middle Fluid Temperature:

$$\lambda_{A,th} = \frac{T_{th,M}^+}{T_{th,P}^+}, \quad \lambda_{B,th} = \frac{\left.\frac{\partial T_{th}^+}{\partial t}\right|_M}{\left.\frac{\partial T_{th}^+}{\partial t}\right|_P}$$

Thermocline Centerline Middle Fluid Density:

$$\lambda_{A,\rho} = \frac{T_{\rho,M}^+}{T_{\rho,P}^+}, \quad \lambda_{B,\rho} = \frac{\left.\frac{\partial T_{\rho}^+}{\partial t}\right|_M}{\left.\frac{\partial T_{\rho}^+}{\partial t}\right|_P} \tag{39}$$

Inlet Fluid Temperature:

$$\lambda_{A,in} = \frac{T_{in,M}^+}{T_{in,P}^+}, \quad \lambda_{B,in} = \frac{\left.\frac{\partial T_{in}^+}{\partial t}\right|_M}{\left.\frac{\partial T_{in}^+}{\partial t}\right|_P}$$

Outlet Fluid Temperature:

$$\lambda_{A,out} = \frac{T_{out,M}^+}{T_{out,P}^+}, \quad \lambda_{B,out} = \frac{\left.\frac{\partial T_{out}^+}{\partial t}\right|_M}{\left.\frac{\partial T_{out}^+}{\partial t}\right|_P}$$

Wall Temperature:

$$\lambda_{A,w} = \frac{T_{w,M}^+}{T_{w,P}^+}, \quad \lambda_{B,w} = \frac{\left.\frac{\partial T_{w}^+}{\partial t}\right|_M}{\left.\frac{\partial T_{w}^+}{\partial t}\right|_P}$$

Inlet Velocity:
$$\lambda_{A,v_z} = \frac{v_{z,M}^+}{v_{z,P}^+}, \quad \lambda_{B,v_z} = \frac{\left.\frac{\partial v_z^+}{\partial t}\right|_M}{\left.\frac{\partial v_z^+}{\partial t}\right|_P}$$

Ambient Temperature:
$$\lambda_{A,amb} = \frac{T_{amb,M}^+}{T_{amb,P}^+}, \quad \lambda_{B,amb} = \frac{\left.\frac{\partial T_{amb}^+}{\partial t}\right|_M}{\left.\frac{\partial T_{amb}^+}{\partial t}\right|_P}$$

After thorough investigation, several types of phase space coordinate transformations were considered, leading to the selection of ω-strain type scaling (shown in Table 1). Two main factors drove the selection: the time scaling and fluid properties. One of the objectives was to doubly accelerate the thermal charge and discharge of the TTSS. To achieve this goal, the timing of the projected transient data must be half of the measured data and eliminates the dilation and identity phase space transformations due to restricting the time ratio to be 1.

Based on equations shown in Equations (31), (33), and (37), the following are the non-dimensionalized, model and prototype divided, law of scaled ratios applied, and inserted with expressions shown in Equation (38):

Mass Conservation:
$$\lambda_{B,\rho} = \left(\frac{v_{z,0}}{\Delta z_0}\right)_R \left(\frac{\lambda_{A,v_z}\lambda_{A,\rho}}{\lambda_{A,z}}\right) \tag{40}$$

$$\lambda_{B,v_z} = \frac{\lambda_{A,v_z}\lambda_{B,\rho}}{\lambda_{A,\rho}}, \lambda_{B,v_z} = \left(\frac{P_0}{\rho_0 v_{z,0}\Delta z_0}\right)_R \frac{\lambda_{A,P}}{\lambda_{A,\rho}\lambda_{A,z}},$$

Momentum Conservation: (41)

$$\lambda_{B,v_z} = \left(\frac{\nu}{R^2}\right)_R \left(\frac{\lambda_{A,z}}{\lambda_{A,r}^2}\right)$$

$$\lambda_{B,th} = \left(\frac{\rho_{in}R_{in}^2 v_{z,in,0}c_{P,in}}{\rho_{th}c_{P,th}R_{th}^2\Delta z}\right)_R \lambda_{A,v_{z,in}}\lambda_{A,th},$$

$$\lambda_{B,th} = \left(\frac{\rho_{in}R_{in}^2 v_{z,in,0}c_{P,th}T_{in,0}}{\rho_{th}c_{P,th}R_{th}^2\Delta z T_{th,0}}\right)_R \lambda_{A,v_{z,in}}\lambda_{A,in},$$

Energy Conservation:
$$\lambda_{B,th} = \left(\frac{\rho_{in}R_{in}^2 v_{z,in,0}c_{P,th}T_{out,0}}{\rho_{th}c_{P,th}R_{th}^2\Delta z T_{th,0}}\right)_R \lambda_{A,v_{z,in}}\lambda_{A,out}, \tag{42}$$

$$\lambda_{B,th} = \left(\frac{kT_{w,0}}{\rho_{th}c_{P,th}\varepsilon R_{th}^2 T_{th,0}}\right)_R \frac{\lambda_{A,w}}{\lambda_{A,r}},$$

$$\lambda_{B,th} = \left(\frac{kT_{w,amb}}{\rho_{th}c_{P,th}\varepsilon R_{th}^2 T_{th,0}}\right)_R \frac{\lambda_{A,amb}}{\lambda_{A,r}}$$

Two other objectives were to maintain geometry and conserve the amount of heat stored during the transients. Considering all geometric ratio terms are 1, and the projected ambient temperature environment is expected to be equivalent to the prototype, the corresponding scaling ratios are shown in Equation (42) (thermocline centerline middle fluid density has been converted to inlet density):

$$
\begin{aligned}
&\text{Thermocline Height:} && \lambda_{A,z} = 1,\ \ \lambda_{B,z} = \frac{1}{t_R} \\
&\text{Thermocline Radius:} && \lambda_{A,r} = 1,\ \ \lambda_{B,r} = \frac{1}{t_R} \\
&\text{Thermocline Centerline Middle Fluid Temperature:} && \lambda_{A,r} = \left(\frac{k}{\rho_{th} c_{P,th} T_{th,0}}\right)_R \frac{1}{t_R} \\
&\text{Thermocline Centerline Middle Fluid Density (results in thermocline fluid velocity):} && \lambda_{A,v_{th}} = \frac{1}{\left(v_{z,0}\right)_R t_R},\ \ \lambda_{B,v_{th}} = \frac{1}{\left(v_{z,0}\right)_R t_R^2} \\
&\text{Inlet Fluid Temperature:} && \lambda_{A,in} = \left(\frac{c_{P,in} k}{\rho_{th} c_{P,th}^2 T_{in,0}}\right)_R \frac{1}{t_R},\ \ \lambda_{B,in} = \left(\frac{c_{P,in} k}{\rho_{th} c_{P,th}^2 T_{in,0}}\right)_R \frac{1}{t_R^2} \\
&\text{Outlet Fluid Temperature:} && \lambda_{A,out} = \left(\frac{\rho_{out} c_{P,th}}{\rho_{th} c_{P,th}^2 T_{out,0}}\right)_R \frac{1}{t_R},\ \ \lambda_{B,out} = \left(\frac{\rho_{out} c_{P,th}}{\rho_{th} c_{P,th}^2 T_{out,0}}\right)_R \frac{1}{t_R^2} \\
&\text{Wall Temperature:} && \lambda_{A,w} = \left(\frac{1}{T_{w,0}}\right)_R,\ \ \lambda_{B,w} = \left(\frac{1}{T_{w,0}}\right)_R \frac{1}{t_R} \\
&\text{Inlet Velocity:} && \lambda_{A,v_z} = \left(\frac{\rho_{th} c_{P,th}}{\rho_{in} c_{P,in}}\right)_R t_R,\ \ \lambda_{B,v_z} = \left(\frac{\rho_{th} c_{P,th}}{\rho_{in} c_{P,in}}\right)_R \\
&\text{Ambient Temperature:} && \lambda_{A,amb} = 1,\ \ \lambda_{B,amb} = \frac{1}{t_R}
\end{aligned}
\tag{43}
$$

For the remainder of coordinate transfer methods, Equation (42) dictated their elimination by parametrically testing applicable thermocline, inlet, and outlet fluid properties, including wall properties. The study revealed β-strain scaling could not produce a time ratio lower than 0.6 (i.e., the heat storage can only be accelerated up to 67%) while staying within the bounds of reasonable temperatures. For 2-2 affine (as shown in Table 1, λ_A and λ_B values are not restricted to any value), valid scaling ratios turned out to be multiples of the ω-strain scaling (i.e., ratios were $\lambda_A : \lambda_B = n : 2n$, where n is any positive real number) and in essence did not provide unique scaling information. The scaling results for reference values to normalize the generated and projected data is provided in Table 2 and Table 3.

Table 2. Prototypic reference values used to normalize parameters of interest *[20]*.

Prototype Scaling Parameter	Values
Thermocline Fluid Reference Temperature	166°C
Thermocline Fluid Reference Density	909.4 kg/m^3
Thermocline Fluid Reference Specific Heat	2.0716 kJ/(kg·K)
Charge Line Reference Temperature	196°C
Charge Line Reference Density	887.98 kg/m^3
Charge Line Reference Specific Heat	2.1802 kJ/(kg·K)
Discharge Line Reference Temperature	187°C

Prototype Scaling Parameter	Values
Wall Reference Temperature	194°C
Wall Reference Conductive Heat Transfer Coefficient	15.7 W/(m·K)
Inlet Reference Velocity	0.458 m/s

Table 3. Projected reference values used to normalize parameters of interest *[20]*.

Projected Scaling Parameter	Values
Thermocline Fluid Reference Temperature	354°C
Thermocline Fluid Reference Density	762.5 kg/m^3
Thermocline Fluid Reference Specific Heat	2.7813 kJ/(kg·K)
Charge Line Reference Temperature	417.78°C
Charge Line Reference Density	707.97 kg/m^3
Charge Line Reference Specific Heat	3.0367 kJ/(kg·K)
Discharge Line Reference Temperature	398.59°C
Wall Reference Temperature	413.51°C
Wall Reference Conductive Heat Transfer Coefficient	18.9 W/(m·K)
Inlet Reference Velocity	0.455 m/s

To satisfy the conservation of stored energy, the utilization of the ω-strain scaling method and parametrically derived nominal values ensures near-ideal conditions. The exact ideal conditions, although the requirements are known, could not be produced in this analysis due to the variability of fluid and material properties at different temporal temperatures. Since each scaling ratio is about the temperature, specific heat, and density of therminol 66 (stainless steel for tank walls), the possible value combinations restrict the achievable agents of change (ω) scaling ratio (λ_B) values. The ω-strain coordinate transformation restricts the parameter of interest (β) scaling ratio (λ_A) value to 1. The ideal value would be 2 where the time ratio is 0.5. As shown in Table 4, the thermocline centerline middle fluid temperature agents of change are slightly less than the ideal value of 2. One aspect of Table 4 is that other parameters' scaling ratios are not exactly ω-strain scaling. Recalling that the objective is to conserve the heat storage, the ω-strain is only applied to the thermocline centerline middle fluid temperature. The rest of the terms change scaling ratios to enforce near-ideal scaling for the main parameter of interest and retroactively attain 2-2 affine coordinate transformation. The behaviors observed accelerating the base case are represented in sections below.

Table 4. Scaling ratio values used to attain a doubly accelerated energy charge and discharge *[20]*

Parameters	λ_A	λ_B
T_{th}	1.000	1.993
T_{in}	1.037	2.069
T_{out}	1.027	2.046
T_w	0.4692	0.9351
v_{in}	0.5086	1.014

4.2.3 Base Case and Projected Case Comparison

The TEDS facility conducted tests to observe the charging and discharging modes for a thermocline storage system in TEDS. The thermocline was charged until the system reached the desired target temperature. It then switched to discharging mode to remove excess heat. The temperature and velocity data were analyzed to determine the β, ω, ω' (first derivative of agents of change), and D parameters and the temperature, and velocity data were then normalized with the nominal values listed in Table 2 and Table 3.

4.2.3.1 Thermocline Centerline Middle Fluid Temperature

The temperature data were analyzed in locations that were representative of the thermocline inlet, outlet, and centerline positions. The data were smoothed using a Savitzky–Golay filter to reduce noise. Figure 6 shows the normalized centerline thermocline temperature trace for the duration of the test, with both operation modes listed as well.

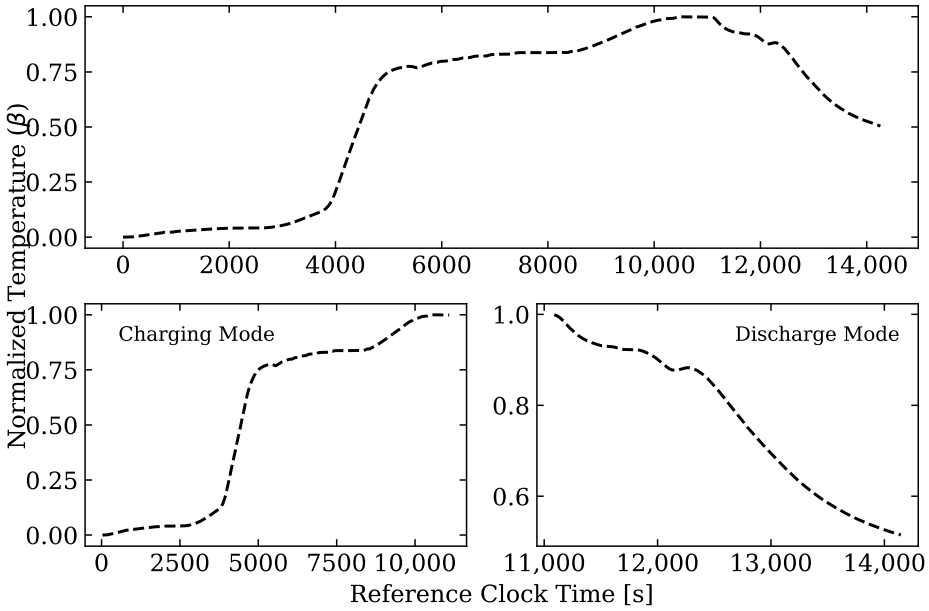

Figure 6. Normalized temperature data from the thermocline centerline location: reference is $T_0 = 418$°C [20].

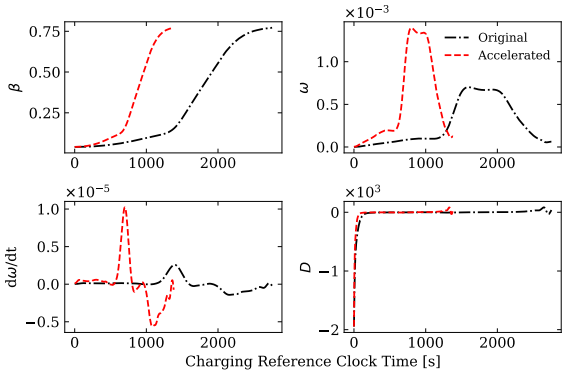

Figure 7. Scaling comparison of charging mode at the centerline, phase 1 [20]

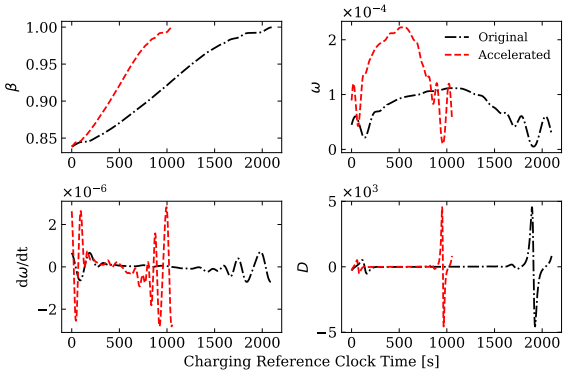

Figure 8. Scaling comparison of charging mode at the centerline, phase 2 [20].

Because local equilibrium points create singularities in DSS, each mode was separated into individual regions of interest to avoid this issue, shown in Figure 7 and Figure 8 for the charge mode, and Figure 9 and Figure 10 for the discharge mode. The centerline charging mode analysis was separated into two phases due to the presence of a local equilibrium position that was reached in charging mode between roughly 5000 (s) < t < 8000 (s), as seen in Figure 6. Figure 7 and Figure 8 show the β (normalized raw data), ω (first derivative of β), ω' (first derivative of ω or second derivative of β), and D (second-order term, also known as the temporal displacement rate) values for the original measured data and the scaled data from using the λ_A = 1.000 and λ_B = 1.993 values, which corresponded to a process time ratio of τ_R= 0.502. The accelerated data occurred in roughly half the time of the original charging sequence. For a simpler visualization of this, the reference time is presented as the relative reference time passed. Each projected point was 0.502 of the past data time, but at different magnitudes that were not consistent with the time ratio. This was due to the scaling ratios derived in Section 4.2.2, in which the scaling was non-linear to the time ratio and was fluid property-dependent. An important aspect of using the ω-strain scaling is that the scaled and original data sets need to have equivalent temporal displacement rates. When the x-axis was given as fractions of the maximum time, it could be seen that this requirement was achieved and that the two processes were invariant.

The thermocline discharge data were similarly analyzed using the same λ_A, λ_B, and τ_R values from Figure 7 and Figure 8 to construct the accelerated data set. Similar to the charging mode, a period of equilibrium was reached between the reference time of 11,500 (s) < t < 12,000 (s), which required the discharge data to be split into two analysis phases. Figure 9 and Figure 10 show the main DSS parameters for each phase in discharging mode. The magnitude agreement between the temporal displacement rates were maintained and the transient features of both the ω and ω' parameters were seen to be magnified in the accelerated case. The temporal displacement rate changed sign twice during the first phase, indicating that the discharge process switched from a dilated process time interval to a contracted process time interval and then back to dilated. In other words, the relative change between the reference time and process time shifted in magnitude, which displayed the complexity of the data geometry.

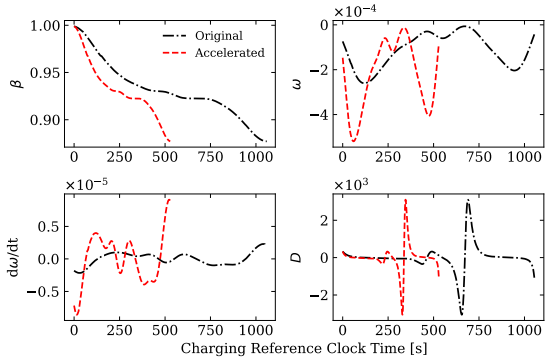

Figure 9. Scaling comparison of discharging mode at the centerline, phase1 [20].

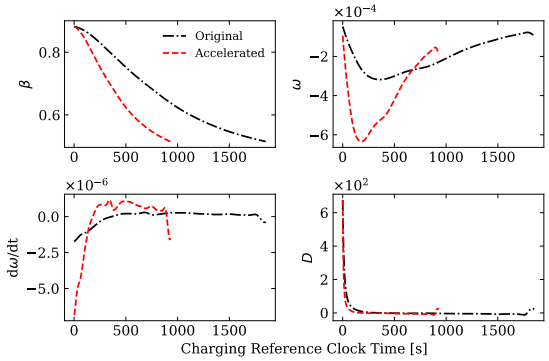

Figure 10. Scaling comparison of discharging mode at the centerline, phase 2 [20].

The scaled process curves for both modes in Figure 11 and Figure 12 show that there was an overlap between the curves, indicating that the ω-strain scaling was successfully applied to the data and that there was no distortion within the thermocline temperature data. This represented the required temperature transient, and the first- and second-order effects that were needed to maintain no distortion and allow the thermocline to be charged and discharged twice as a fast in this specific test. If the TEDS facility were to design a future experiment for half-time but desired the same amount of stored energy, it is expected that the generated data would follow the accelerated data by using the given boundary conditions at the times derived by DSS. This projection of data would support the signal conversion for incoming and outgoing information for DETAIL.

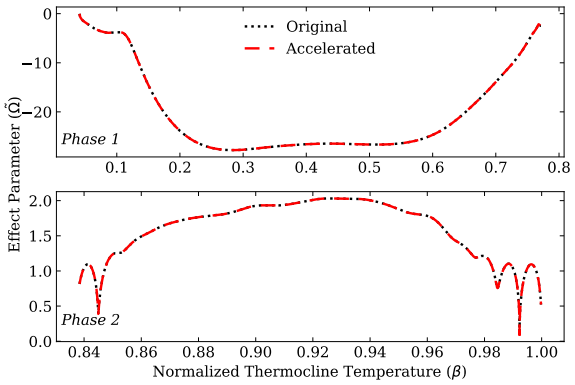

Figure 11. Normalized Charge Mode Thermocline Temperature [20].

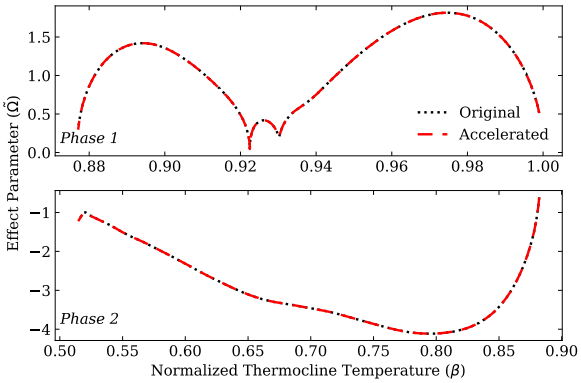

Figure 12. Normalized Discharge Mode Thermocline Temperature [20].

4.2.3.2 Charge Line Temperature

The normalized inlet temperature traces are shown in Figure 13, with data separated for the charging and discharging modes provided as well. In Figure 13, it can be seen that there were several periods of temperature plateau, which limited the data regions that were available for the DSS analysis. For the inlet location, the $\lambda_A = 1.037$, $\lambda_B = 2.068$, and resulting $\tau_R = 0.501$ values were not identical to the thermocline centerline λ values, as discussed in Table 4. The change in temperature trends was attributed to the flow direction at different modes. In charging mode, the hot fluid flowed from the thermocline inlet and out of the thermocline outlet. On the other hand, discharging mode injected cold fluid (relatively low temperature compared to the hot fluid temperature) in the thermocline outlet that was then ejected out of the thermocline inlet, thus reversing the flow. This explained the delayed temperature response compared to the thermocline temperatures in Figure 6, as the interface of the cold and hot fluid traveled back to the inlet location.

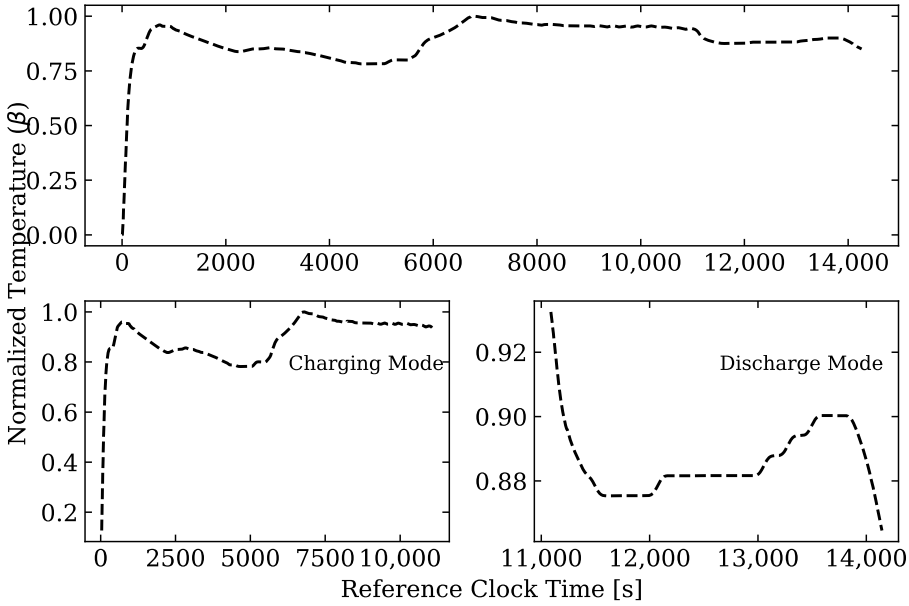

Figure 13. Normalized temperature data from the thermocline inlet location: reference is $T_0 = 354°C$ [20].

The charging mode data for the inlet location needed to be separated into two phases, similar to the previous sections. As expected, the charging data saw a temperature plateau region that was similar to that observed in the thermocline centerline data. The DSS parameters for both phases are plotted in Figure 14 and Figure 15, in which it can be seen that the temporal displacement rates were equivalent once again. However, because the λ_A value was not exactly 1.0, the beta traces were slightly offset in magnitude. This offset was most observable in the second phase, for which it was analyzed over a short time interval.

The DSS parameters for the discharge mode thermocline inlet location are shown in Figure 16 and Figure 17. Similarly, trends were observed in the matched temporal displacement rates, indicating that the process time intervals were matched between the original and scaled accelerated scenarios. Additionally, the features of the ω and ω' terms were magnified by the accelerated case, as expected. The shift in β values appeared to be magnified due to the short time interval that was considered for the discharge phasing and the axis limits.

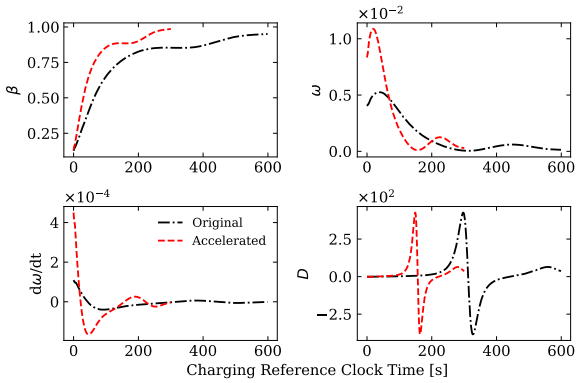

Figure 14. Comparison of charging mode at the inlet location, phase 1 [20].

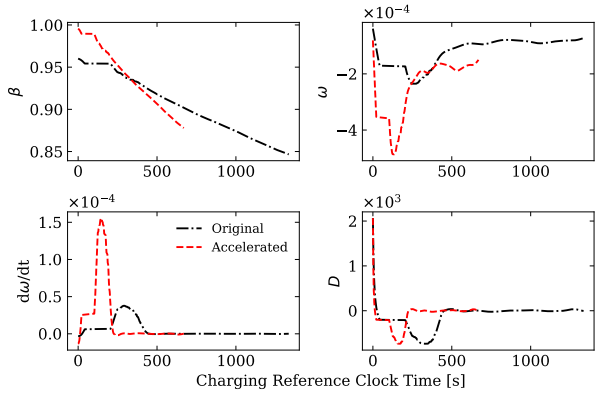

Figure 15. Comparison of charging mode at the inlet location, phase 2 [20].

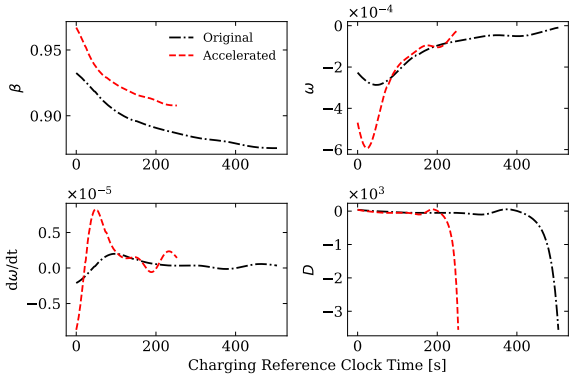

Figure 16. Comparison of discharging mode at the inlet location, phase 1 [20].

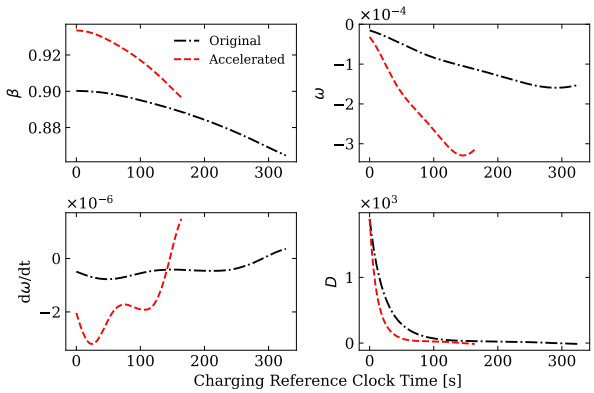

Figure 17. Comparison of discharging mode at the inlet location, phase 2 [20].

The comparison of the scaled process curves in Figure 18 and Figure 19 shows that curve separation occurred in both modes. This was expected because the λ_A value was not exactly 1.0 and the shift of the curve was more prominent in the discharge phase, primarily due to the short time interval that was used for the analysis, which emphasized the separation more. In the first mode, the separation became more pronounced as the charging phase evolved. This showed that slight deviations from the ω-strain requirement of $\lambda_A = 1$ could result in a process being scaled more by 2–2 affine scaling. However, the matched $\widetilde{\Omega}$ magnitudes indicated that the transient aspect of the process time was preserved between the two cases. If the effect parameter values and normalized thermocline temperatures were to be divided by their corresponding scaling ratios of $\lambda_A = 1.037$, the data points would overlap perfectly, which is an indication of perfect similitude.

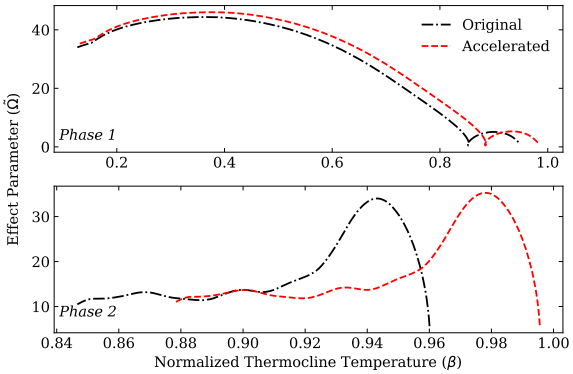

Figure 18. Charge line normalized inlet temperature (β) [20].

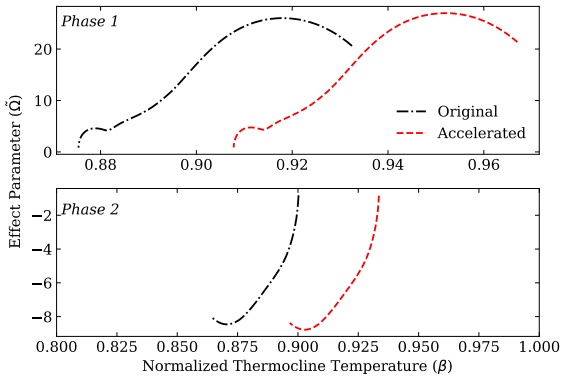

Figure 19. Discharge line normalized inlet temperature (β) [20].

4.2.3.3 Discharge Line Outlet Temperature

The normalized thermocline outlet temperature data and reference values used for the normalization are shown in Figure 20, along with the separated data that were considered in the charging and discharging mode analysis. Compared to the inlet location, the charging data had a similar temperature plateau region, which also required the charging data to be analyzed in two phases. However, the discharging mode data recorded a substantially smoother temperature decrease without the plateau regions that were seen in the two other locations. This resulted in the discharging mode data being analyzed in one data set. Due to the flow reversal during mode transitions, the timing of the trend changes was quicker than that of the thermocline centerline and inlet temperatures.

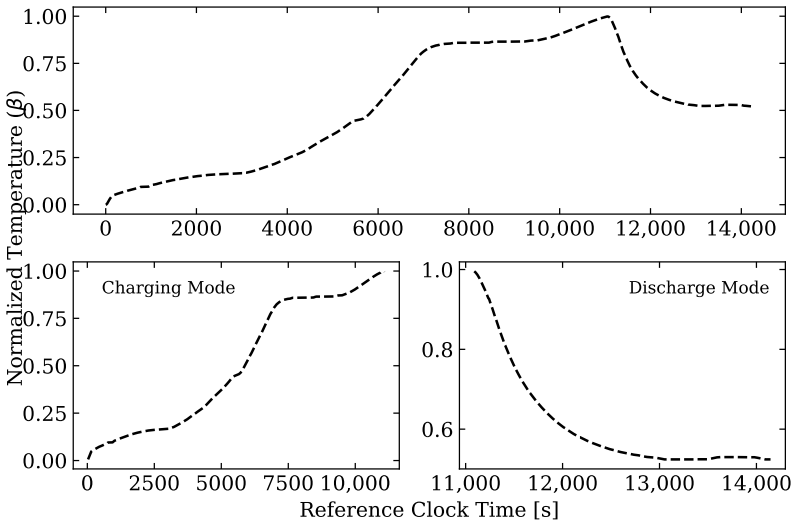

Figure 20. Normalized temperature data from the thermocline outlet location: reference is $T_0 = 414°C$ [20].

The β values presented in Figure 21 and Figure 22 show that the 2–2 affine scaling for the outlet location (λ_A = 1.027) required the scaled data set to a have a slightly higher normalized outlet temperature than that of the original test. However, because the temporal displacement was preserved, the transient process time similitude was maintained. Since the scaling ratio was different from that at the thermocline inlet ($\lambda_{A,inlet}$ = 1.037 > $\lambda_{A,outlet}$ = 1.027), the displacements shown in Figure 21 and Figure 22, and Figure 14 and Figure 15 were not equivalent. Again, these differences in scaling ratios were a product of the DSS derivations, based on physics relationships and fluid properties. If other constraints were to exist, the difference would potentially be larger but would not affect the accuracy of the projection.

The DSS parameters for the discharge thermocline outlet location are plotted in Figure 23, which did not experience the temperature plateau regions that were observed in the inlet location data. As with the other results, it was observed that the temporal displacement rate was preserved in the accelerated case, as required for the scaling type. The accelerated ω' had to be larger than the original data by a scale factor of λ_A^2/λ_B, which resulted from substituting Equation (13) and (14) into the definition of ω'. Since the time ratio ($\tau_R = \lambda_A/\lambda_B$) was equivalent for all parameters and locations, the timing was always roughly half of that of the original data. It was the determination of the magnitude of each temporal data point that produced the DSS data projection value.

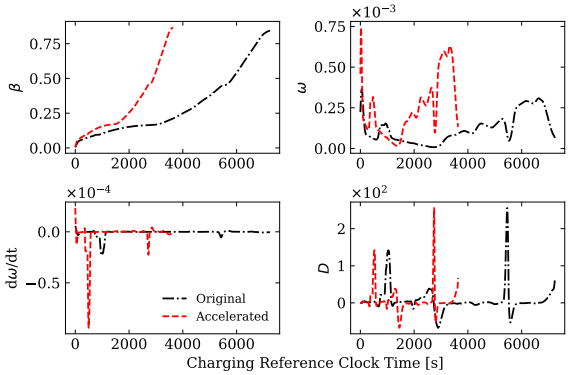

Figure 21. Comparison of charging mode at the outlet location, phase 1 [20].

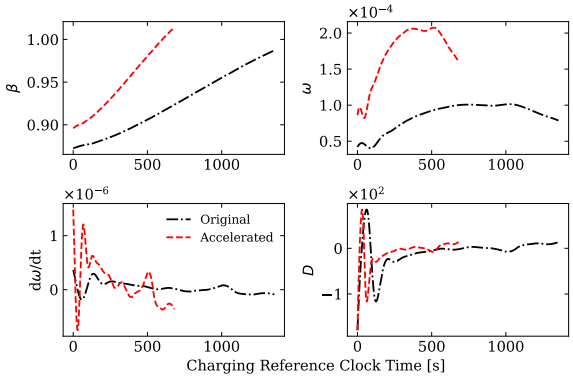

Figure 22. Comparison of charging mode at the outlet location, phase 2 [20].

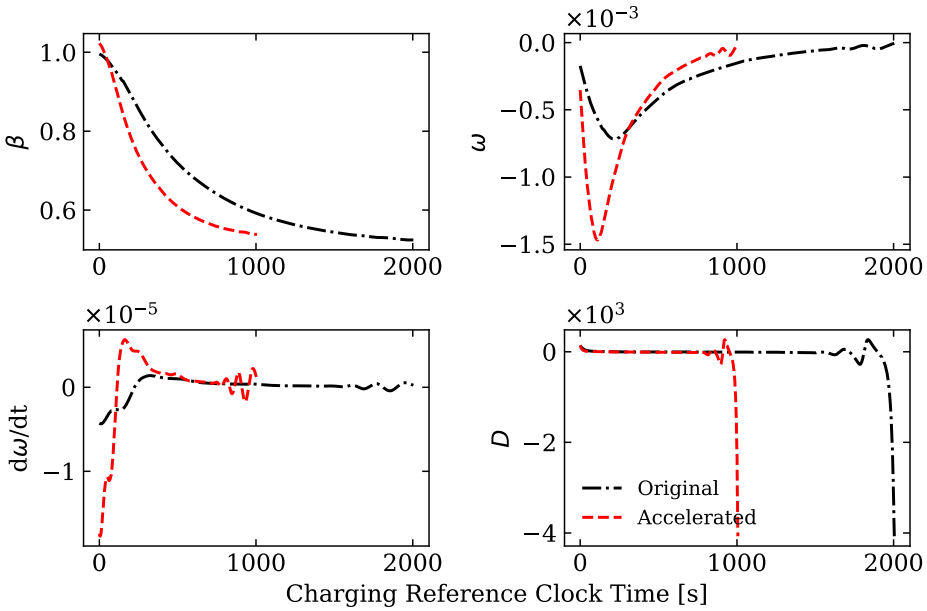

Figure 23. Comparison of discharging mode at the outlet location [20].

The scaled process curve of the first phase (shown in Figure 24) shows that there was very minimal separation between the two data sets. The separation distance became more pronounced as the outlet temperature increased toward its maximum value for the first phase. The separation was more pronounced in the second phase, primarily due to the small axis limits for the figure, and the differences of 2.07% became more apparent at higher β values. As noted in the inlet case, the accelerated case required the normalized temperature to be slightly larger than that of the original case. It should be noted that the separation was not a result of the derivation but was recognized as the necessary change in the phase space ($\widetilde{\Omega} - \beta$) to guarantee the perfect overlap of the thermocline temperatures

The comparison of the scaled process curves presented in Figure 25 shows that the magnitudes of the normalized temperature rates of change ($\widetilde{\Omega}$) were maintained across discharging mode. This indicates that the process action and ω term were correctly scaled to preserve the process similitude. A similar β shift was seen for the accelerated data because of $\lambda_A = 1.027$, with the separation becoming more pronounced at higher β values, which was at the beginning of the operation mode.

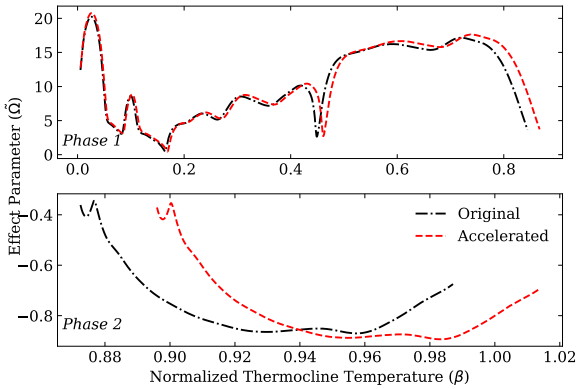

Figure 24. Scaled process curves of charging mode at the outlet location [20].

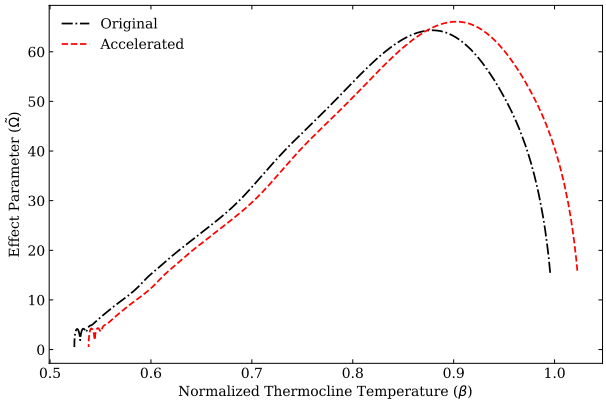

Figure 25. Scaled process curves of discharging mode at the outlet location [20].

4.2.3.4 Discharge Mode Inlet Velocity

The velocity data were determined from two inline flowmeters located on the outlet side of the thermocline system. Each operation mode (charging-discharging) has a dedicated flow path that branches out from the system's main outlet piping. Because of the flow paths and the operation control configuration of the thermocline system, when one operation mode is active, there is no fluid flow through the flow path of the other operation mode. Due to the high noise and oscillating values for the velocity that were determined from the flowmeter FM-202 for the charging mode, an analysis was not performed on the charging mode velocity. A limitation of DSS is the difficulty in analyzing the oscillating data. While some data reach natural equilibrium when a process undergoes a shift in behavior (such as reaching a peak temperature), oscillating data primarily indicate that the instrument is having difficulty collecting a smooth signal. The $\lambda_A = 0.5086$ and $\lambda_B = 1.014$ values that were used to scale the data were taken from Table 4 and applied to discharging mode. In contrast to the inlet and outlet locations, the velocity scaling ratio was significantly lower than the thermocline centerline temperature. This was due to the inverse proportional relationship of the energy-governing equation against the proportional relationships of the inlet and outlet temperatures:

$$\lambda_{B,T} \approx \lambda_{A,v_z}\lambda_{A,T} \approx \frac{\lambda_{A,inlet,outlet}}{\lambda_{A,T}} \tag{44}$$

If the system acceleration were set to more than double, the velocity scaling ratio would potentially drop to lower values. The discharging mode data were analyzed from flowmeter FM-201 and the normalized flow velocity is plotted in Figure 26. Because several local velocity equilibrium points were reached in discharging mode, four separate phases were analyzed within the data set to complete the DSS analysis.

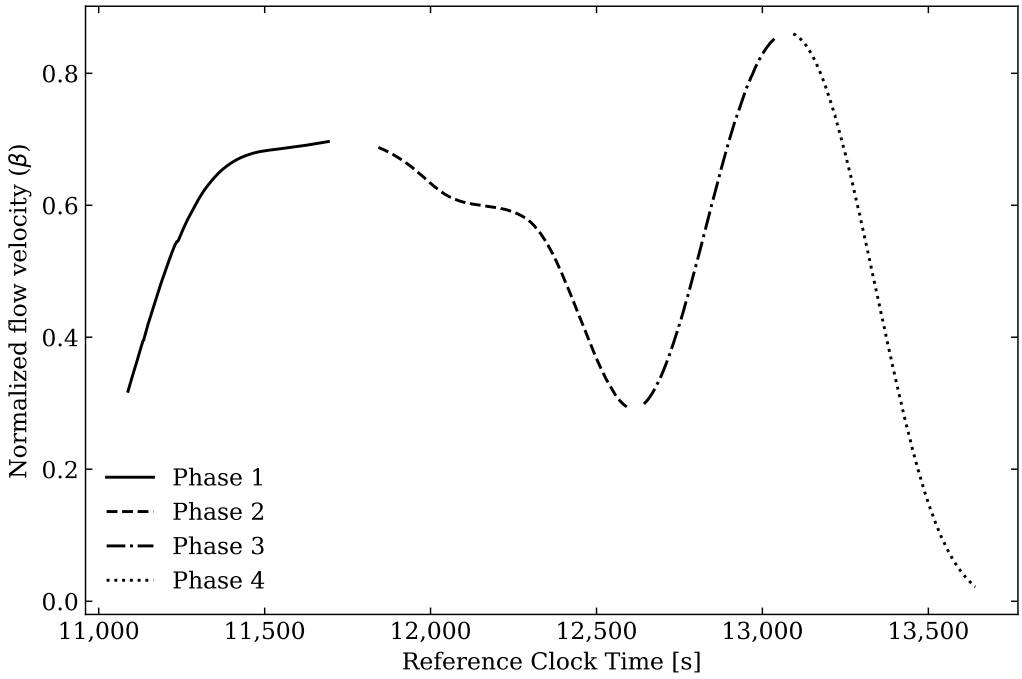

Figure 26. Normalized flow velocity data from discharging mode [20].

Figure 27 shows the scaled process curves for all four phases of discharging mode, in which several features can be observed. First, both the β and $\widetilde{\Omega}$ accelerated values shifted from the original data. The β values were roughly halved, based on the $\lambda_A \approx 0.5$ parameter. Because the λ_B value was close to 1, the flow velocity was scaled by the β-strain scaling type, as described in Table 1. This resulted in a shift toward the $\widetilde{\Omega}$ values by a factor of λ_A. Regardless of the observed shifts in data, the data geometry remained identical, which was evidence of the conserved physics. This highlighted that preserving the process similitude in the temperature response corresponded to projections being further away, which resembled a different scaling mode for the flow velocity. This result suggested that scaled systems are able to perfectly preserve every parameter response without the introduction of scaling distortion, as long as the governing equations capture the true agents of change. If any dominating agent of change were missing, the determined projection would potentially be invalid. However, this is not a weakness of the DSS methodology, but rather a strength since the detection of missing physics is helpful in the theoretical modeling of observed phenomena.

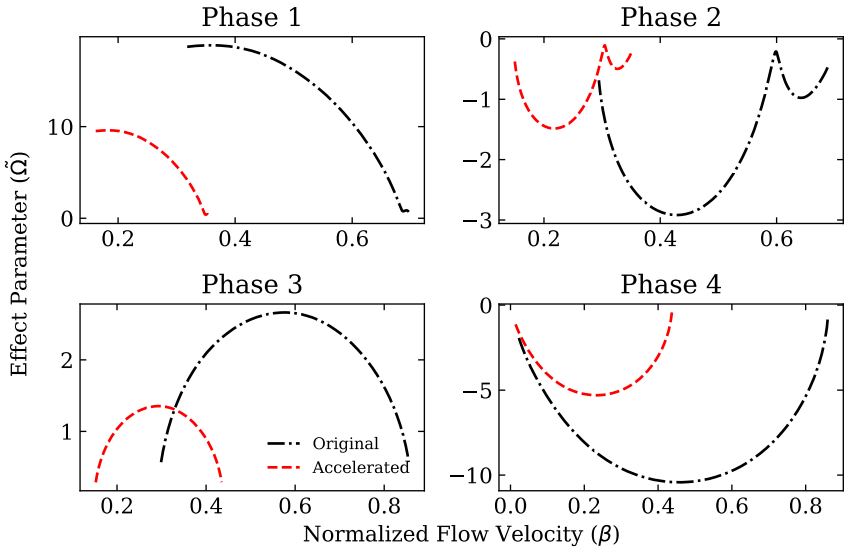

Figure 27. Scaled process curves of the flow velocity in discharging mode [20].

4.3 Thermal Energy Distribution System Hierarchal Two-Tiered Scaling

The TEDS TTSS H2TS activity was initiated after the completion of the DSS work in Section 4.2, and was not completed before the last milestone. The content shown for this section will be a detailed description of the process to achieve the doubly accelerated heat storage conserved system based on previously run data.

4.3.1 Non-Dimensionalization of Thermal Energy Distribution System Conservation Laws

As similarly stated in Section 4.2.1, the following steps are required complete the data projection: (1) non-dimensionalize governing laws, (2) derive residence time and characteristic time ratio for each governing law, (3) determine projected nominal conditions to keep scaled characteristic time ratio groups equivalent to the base case, and (4) balance relations to ensure the projected residence time is half of the base case. The reference point to normalize each parameter is the mode transition time point.

4.3.2 Conservation of Mass

The following are the relations to normalize each parameter by the selected reference data point:

$$\rho_{th}^{+} = \frac{\rho_{th}}{\rho_{th,0}},\ v_z^{+} = \frac{v_z}{v_{z,0}},\ z^{+} = \frac{z}{\Delta z_0} \tag{45}$$

From Equation (45), non-dimensionalize the conservation of mass:

$$\left(\frac{\Delta z_0}{v_{z,0}}\right)\frac{\partial \rho_{th}^{+}}{\partial t} = -v_z^{+}\frac{\partial \rho_{th}^{+}}{\partial z^{+}} - \rho_{th}^{+}\frac{\partial v_z^{+}}{\partial z^{+}} \tag{46}$$

The mass residence time and characterized time ratio are:

$$\tau_{RS,mass} = \frac{\Delta z_0}{v_{z,0}}, \text{no groups produced} \tag{47}$$

4.3.3 Conservation of Momentum

The following are the relations to normalize each parameter by the selected reference data point:

$$\rho_{th}^{+}=\frac{\rho_{th}}{\rho_{th,0}},\ v_{z}^{+}=\frac{v_{z}}{v_{z,0}},\ z^{+}=\frac{z}{\Delta z_{0}},\ P^{+}=\frac{P}{P_{0}},\ r^{+}=\frac{r}{R} \tag{48}$$

Using equations from (33) to (45), non-dimensionalize the conservation of momentum:

$$\left(\frac{R^{2}}{\nu}\right)\frac{\partial v_{z,th}^{+}}{\partial t}=-\left(\frac{R^{2}}{\nu}\right)\frac{v_{z,th}^{+}}{\rho_{th}^{+}}\frac{\partial \rho_{th}^{+}}{\partial t}-\left(\frac{P_{0}R^{2}}{v_{z,0}\nu\rho_{th,0}\Delta z_{0}}\right)\frac{1}{\rho_{th}^{+}}\frac{\partial P^{+}}{\partial z^{+}}+\left(\frac{1}{r^{+}}\frac{\partial v_{z,th}^{+}}{\partial r^{+}}+\frac{\partial^{2}v_{z,th}^{+}}{\partial r^{+2}}+\frac{\partial^{2}v_{z,th}^{+}}{\partial z^{+2}}\right) \tag{49}$$

The momentum residence time and characterized time ratio are:

$$\tau_{RS,momentum}=\frac{R^{2}}{\nu},\Pi_{1}=\frac{P_{0}R^{2}}{v_{z,0}\nu\rho_{th,0}\Delta z_{0}} \tag{50}$$

Given the expression of characteristic time ratio Π_1, it can be denoted as the thermocline internal force ratio where the numerator is the static pressure force and the denominator is the dynamic pressure force.

4.3.4 Conservation of Energy

The following are the relations to normalize each parameter by the selected reference data point:

$$\rho_{th}^{+}=\frac{\rho_{th}}{\rho_{th,0}},\quad v_{z,in}^{+}=\frac{v_{z,in}}{v_{z,in,0}},\quad z^{+}=\frac{z}{\Delta z_{0}},\quad \varepsilon^{+}=\frac{\varepsilon}{\varepsilon_{0}},\quad r^{+}=\frac{r}{R},$$

$$c_{P,th}^{+}=\frac{c_{P,th}}{c_{P,th,0}},\quad R_{in}^{+}=\frac{R_{in}}{R_{in,0}},\quad \rho_{in}^{+}=\frac{\rho_{in}}{\rho_{in,0}},\quad T_{th}^{+}=\frac{T_{th}}{T_{th,0}},\quad h_{c}^{+}=\frac{h_{c}}{h_{c,0}}, \tag{51}$$

$$S_{r}^{+}=\frac{S_{r}}{S_{r,0}},\quad T_{r}^{+}=\frac{T_{r}}{T_{r,0}},\quad k^{+}=\frac{k}{k_{0}},\quad T_{w}^{+}=\frac{T_{w}}{T_{w,0}}$$

Using equations from (37) to (45), non-dimensionalize the conservation of energy:

$$\begin{aligned}\left(\frac{\rho_{th,0}\varepsilon_{0}R^{2}\Delta z_{0}}{\rho_{in,0}v_{z,in,0}}\right)\frac{\partial T_{th}^{+}}{\partial t}= &\ \frac{\rho_{in}^{+}R_{in}^{+2}v_{z,in}^{+}}{\rho_{th}^{+}c_{P,th}^{+}R_{th}^{+2}}\left(T_{th}^{+}\frac{\partial c_{P,th}^{+}}{\partial z^{+}}+c_{P,th}^{+}\frac{\partial T_{th}^{+}}{\partial z^{+}}\right)\\ &+\left(\frac{h_{c,0}S_{r,0}\Delta z_{0}T_{r,0}}{\rho_{in,0}v_{z,in,0}R_{in,0}^{2}c_{P,th,0}T_{th,0}}\right)\frac{h_{c}^{+}S_{r}^{+}T_{r}^{+}}{\rho_{th}^{+}c_{p,th}^{+}\varepsilon^{+}R_{th}^{+2}}\\ &-\left(\frac{h_{c,0}S_{r,0}\Delta z_{0}}{\rho_{in,0}v_{z,in,0}R_{in,0}^{2}c_{P,th,0}}\right)\frac{h_{c}^{+}S_{r}^{+}T_{th}^{+}}{\rho_{th}^{+}c_{p,th}^{+}\varepsilon^{+}R_{th}^{+2}}\\ &+\left(\frac{k_{0}\Delta z_{0}T_{w,0}}{\rho_{in,0}v_{z,in,0}R_{in,0}^{2}c_{P,th,0}T_{th,0}}\right)\frac{R_{w}^{+2}}{\rho_{th}^{+}c_{p,th}^{+}\varepsilon^{+}R_{th}^{+2}}\left(\frac{k^{+}}{r^{+}}\frac{\partial T_{w}^{+}}{\partial r^{+}}\right.\\ &\left.+\frac{\partial k^{+}}{\partial r^{+}}\frac{\partial T_{w}^{+}}{\partial r^{+}}+k^{+}\frac{\partial^{2}T_{w}^{+}}{\partial r^{+2}}\right)\end{aligned} \tag{52}$$

The energy residence time and characterized time ratio are:

$$\tau_{RS,energy} = \frac{\rho_{th,0}\varepsilon_0 R^2 \Delta z_0}{\rho_{in,0} v_{z,in,0}}, \Pi_2 = \frac{h_{c,0} S_{r,0} \Delta z_0 T_{r,0}}{\rho_{in,0} v_{z,in,0} R_{in,0}^2 c_{P,th,0} T_{th,0}},$$
$$\Pi_3 = \frac{h_{c,0} S_{r,0} \Delta z_0}{\rho_{in,0} v_{z,in,0} R_{in,0}^2 c_{P,th,0}}, \qquad \Pi_4 = \frac{k_0 \Delta z_0 T_{w,0}}{\rho_{in,0} v_{z,in,0} R_{in,0}^2 c_{P,th,0} T_{th,0}} \tag{53}$$

Given the expression of characteristic time ratios Π_2, Π_3, and Π_4, the following are the physical interpretations: (1) Π_2 is the thermocline filler heat transfer ratio, (2) thermocline fluid heat transfer ratio, and (3) thermocline wall heat transfer ratio. The denominators are the advective heat transfer terms which are common among the three characteristic time ratios.

4.3.5 Scaling Results and Conclusions

As described in Section 3 Equation (25), H2TS scaling is conducted by matching the determined characterized time ratios. In addition, the term that defines the duration of the phenomenon in question, the residence time for the model design will have to be matched for the given time ratio as well depending on research objectives. In the case of doubling the heat storage rate, this requires the following conditions:

$$\tau_{RS,momentum,M} = 0.5\tau_{RS,momentum,P},\ \tau_{RS,energy,M} = 0.5\tau_{RS,energy,P},\ \Pi_{1,M} = \Pi_{1,P},\ \Pi_{2,M} = \Pi_{2,P},$$
$$\Pi_{3,M} = \Pi_{3,P},\ \Pi_{4,M} = \Pi_{4,P} \tag{54}$$

Identically to the parametric study conducted in Section 4.2.2, the combination of fluid and material properties disregarding geometric alteration is limited and only a few instances may satisfy the scaling conditions. Ignoring the assumption not to alter geometry, Table 5 illustrates the optimized results of the parametric study. Unfortunately, without varying the geometry, the derived set of conditions were too restrictive with the given dependency on fluid and material properties.

Table 5. H2TS data projection [20].

Parameter	Value
Momentum Residence Time	0.1672
Energy Residence Time	0.5121
Force Characterized Time Ratio	1.0063
Filler Heat Transfer Characterized Time Ratio	0.9915
Fluid Heat Transfer Characterized Time Ratio	0.9915
Wall Heat Transfer Characterized Time Ratio	1.0041

Energy residence time, force characterized time ratio, filler heat transfer characterized time ratio, fluid heat transfer characterized time ratio, and wall heat transfer characterized time ratio fit well within the criteria defined in [7]. On the other hand, the momentum residence time could not be 0.5 at the same instance as the energy residence time due to the absence of velocity in the denominator. Since the momentum residence time is in units of time, including velocity will introduce unit adjustment issues. H2TS requires all terms to be dimensionless and remaining reference values are part of either the residence time or the characteristic time ratio. To demonstrate the inclusion of velocity, the following must be true:

$$\tau_{RS,momentum} = \frac{\dots}{v_{z,0}} \tag{55}$$

However, since the reference velocity exists primarily in the numerator, the full non-dimensionalized conservation of momentum equation is divided on both sides by $v_{z,0}^2$. This way, another form of the momentum residence time is found:

$$\tau_{RS,momentum} = \frac{R}{v_{z,0}} = \frac{R^3 \rho_{th,0} \varepsilon_0}{\rho_{in,0} v_{z,in,0} R_{in,0}^2} \tag{56}$$

Although the momentum residence time now resembles the energy momentum and both are now capable of being 0.5 in the same instance, this causes severe dependency on the inlet velocity and characterized time ratios can no longer be matched among prototype and model even if geometric alteration is allowed. For this reason, the expressions derived in Equations (46), (49), and (52) have been dictated to be the optimized H2TS results. Table 6 and Table 7 show the determined reference values and geometric information.

Table 6. Prototypic reference values used to normalize governing equations and geometric information [20].

Prototype Scaling Parameter	Values
Thermocline Tank Radius	7.6 m
Thermocline Internal Pressure	25 kPa
Thermocline Fluid Reference Temperature	166°C
Thermocline Fluid Reference Density	909.4 kg/m^3
Thermocline Fluid Reference Specific Heat	2.0716 kJ/(kg·K)
Charge Line Reference Temperature	196°C
Charge Line Reference Density	887.98 kg/m^3
Charge Line Reference Specific Heat	2.1802 kJ/(kg·K)
Discharge Line Reference Temperature	187°C
Wall Reference Temperature	194°C
Wall Reference Conductive Heat Transfer Coefficient	15.7 W/(m·K)
Inlet Reference Velocity	0.458 m/s

Table 7. Projected reference values used to normalize governing equations and geometric information [20].

Projected Scaling Parameter	Values
Thermocline Tank Radius	6.46 m
Thermocline Internal Pressure	312.5 kPa
Thermocline Fluid Reference Temperature	83°C
Thermocline Fluid Reference Density	967.43 kg/m^3
Thermocline Fluid Reference Specific Heat	1.7772 kJ/(kg·K)
Charge Line Reference Temperature	196°C
Charge Line Reference Density	887.90 kg/m^3
Charge Line Reference Specific Heat	2.1798 kJ/(kg·K)
Discharge Line Reference Temperature	187°C
Wall Reference Temperature	133.86°C
Wall Reference Conductive Heat Transfer Coefficient	14.7 W/(m·K)
Inlet Reference Velocity	0.687 m/s

Unlike the calculated DSS model transient data, the projection of the H2TS method is a static point in the evolving system. The parametrically determined model reference values are the projection for the chosen reference point temporal location which is the time when modes transition from charge to discharge. Thus, the projection of the path before and after the reference point are unknown.

5. HIGH-TEMPERATURE ELECTROLYSIS HYDROGEN GENERATION SCALING ANALYSIS

As part of the data projection demonstration cases, the High Temperature Hydrogen Electrolysis (HTSE) facility in DETAIL was scaled based on the same objectives set for the TEDS facility. The following sections describe the physics, scaling process, and results.

5.1 Hydrogen Electrolysis Governing Equations

The theory shown in this section is for an SOEC, which includes three integrated submodules that have been integrated: electrical dynamics, fluid dynamics, and thermal dynamics [21]. Figure28 shows the basic structure of electrolysis experimental setups designed by INL.

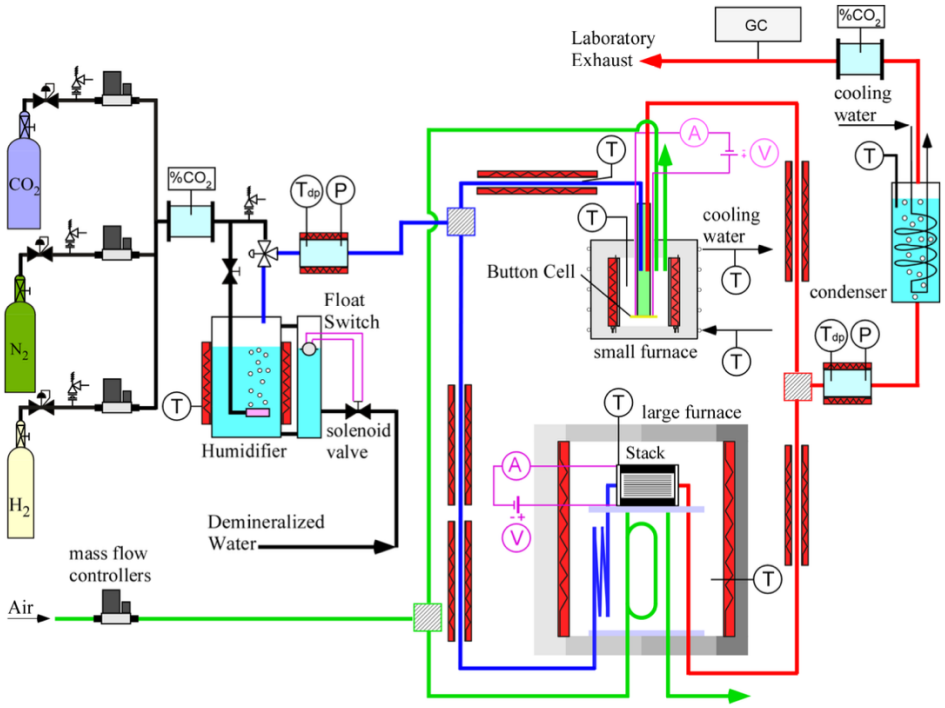

Figure 28. Process flow diagram of the high-temperature electrolysis experimental setup for single-cell and planar stack testing [22].

5.1.1 Electrical Dynamics – Stack Voltage

$$V(I,\bar{T},\bar{P}) = V_{rev}(\bar{T},\bar{P}) + V_{ohm}(I,\bar{T}) + V_{act}(I,\bar{T}) \cdot \frac{1}{1+s\tau_{act}} \tag{57}$$

Where I is the stack current, $\bar{T}$ is the average stack temperature, $\bar{P} = \left[\bar{P}_{H_2O}, \bar{P}_{H_2}, \bar{P}_{O_2}, \bar{P}_{N_2}\right]^T$ are the average partial pressure conditions of the reaction, s denotes the Laplace variable, and τ_{act} is the activation overvoltage time constant. And the first-order delays of τ_{act} arise from the cell's electromechanical double-layer phenomenon.

5.1.1.1 Reversible Overvoltage

According to the Nernst equation, V_{rev} can be further formulated as:

$$V_{rev}(\bar{T},\bar{P}) = V_{oc}(\bar{T}) + \frac{R\bar{T}}{2F}\ln\left(\frac{\bar{P}_{H_2}\bar{P}_{O_2}^{0.5}}{\bar{P}_{H_2O}}\right) \tag{58}$$

Where $R = 8.314$ is the gas constant, and $F = 96485.333$ is the Faraday constant. The open-circuit voltage V_{oc} is associated voltage of Gibbs Free Energy of the reaction:

$$\begin{cases} V_{oc}(\bar{T}) = \frac{\Delta G_R(\bar{T})}{2F} \\ \Delta G_r(T) = 244800 - 49.18 \cdot T - 2.72 \cdot 10^{-3} \cdot T^2 \end{cases} \tag{59}$$

5.1.1.2 Ohmic Overvoltage

The ohmic overvoltage V_{ohm} is attributed to the electrical resistances of the cell structure:

$$V_{ohm}(I,\bar{T}) = I \cdot A \cdot ASR(\bar{T}) \tag{60}$$

Where A is the cell area, and $ASR(\bar{T})$ is the area-specific resistance of the cell obtained from the Arrhenius equation:

$$ASR(\bar{T}) = ASR(T_{ref}) - 0.463 + 3.973 \cdot 10^{-5} \cdot e^{\frac{10300}{\bar{T}}} \tag{61}$$

5.1.1.3 Activation Overvoltage

The activation overvoltage V_{act} denotes the desired voltage to meet the activation energy at both electrodes, which is generally described by the Butler-Volmer equation:

$$V_{act}(I,\bar{T}) = \frac{R\bar{T}}{2F}\left[\sinh^{-1}\left(\frac{I}{2I_{ex,ca}}\right) + \sinh^{-1}\left(\frac{I}{2I_{ex,an}}\right)\right]$$

$$I_{ex,ca} = \frac{R\bar{T}}{2F}\Gamma_{ex,ca}e^{-\frac{\xi_{ca}}{R\bar{T}}}, I_{ex,an} = \frac{R\bar{T}}{2F}\Gamma_{ex,an}e^{-\frac{\xi_{an}}{R\bar{T}}} \tag{62}$$

Where $I_{ex,ca}$ (or $I_{ex,ca}$) is the cathode (or anode) exchange current calculated from the corresponding pre-exponential factor $\Gamma_{ex,ca}$ (or $\Gamma_{ex,an}$) and activation energy ξ_{ca} (or ξ_{an}).

5.1.2 Fluid Dynamics

This submodule outputs the dynamic behavior of the stack average partial pressure conditions $\bar{P} = \left[\bar{P}_{H_2O}, \bar{P}_{H_2}, \bar{P}_{O_2}, \bar{P}_{N_2}\right]^T$ of the reaction and task inlet and outlet flow rate conditions $w_{in} = \left[w_{H_2O,in}, w_{H_2,in}, w_{O_2,in}, w_{N_2,in}\right]^T$, $w_{out} = \left[w_{H_2O,out}, w_{H_2,out}, w_{O_2,out}, w_{N_2,out}\right]^T$ of the stack.

5.1.2.1 Partial Pressure

The average partial pressure conditions of the reaction $\bar{P} = \left[\bar{P}_{H_2O}, \bar{P}_{H_2}, \bar{P}_{O_2}, \bar{P}_{N_2}\right]^T$ can be calculated based on the inlet partial pressure conditions $\bar{P}_{in} = \left[\bar{P}_{H_2O,in}, \bar{P}_{H_2,in}, \bar{P}_{O_2,in}, \bar{P}_{N_2,in}\right]^T$, and the outlet partial pressure conditions $\bar{P}_{out} = \left[\bar{P}_{H_2O,out}, \bar{P}_{H_2,out}, \bar{P}_{O_2,out}, \bar{P}_{N_2,out}\right]^T$:

$$\begin{cases} \bar{P}_{H_2O} = P_{H_2O,in}^{(1-\lambda)} P_{H_2O,out}^{\lambda} \cdot \frac{1}{1+s\tau_{H_2O}} \\ \bar{P}_{H_2} = P_{H_2,in}^{(1-\lambda)} P_{H_2,out}^{\lambda} \cdot \frac{1}{1+s\tau_{H_2}} \\ \bar{P}_{O_2} = P_{O_2,in}^{(1-\lambda)} P_{O_2,out}^{\lambda} \cdot \frac{1}{1+s\tau_{O_2}} \\ \bar{P}_{N_2} = P_{N_2,in}^{(1-\lambda)} P_{N_2,out}^{\lambda} \cdot \frac{1}{1+s\tau_{N_2}} \end{cases} \tag{63}$$

Where $\lambda \in (0,1)$ is a constant selected through parametric studies. It should be noted that $\bar{P}$ is calculated in a geometric manner due to the logarithmic form in the Nernst equation. And the first-order delays of τ_{H_2O}, τ_{H_2}, τ_{O_2}, and τ_{N_2} describes the pressure inertia arises from the finite gas flow rates. Referring to the definition of air ratio for high-temperature fuel cells and electrolyzers, first introduce feed factors π_{ca} and π_{an} to represent the inlet molar flows of both electrodes of the SOEC system:

$$\pi_{ca} = \frac{H_2O \text{ provided in cathode stream}}{H_2O \text{ consumed by electrolysis}} = \frac{w_{H_2O,in}}{\frac{I}{2F}}$$

$$\pi_{an} = \frac{O_2 \text{ provided in anode stream}}{O_2 \text{ consumed by electrolysis}} = \frac{w_{H_2O,in}}{0.5\frac{I}{2F}} \tag{64}$$

In fact, with the inlet composition fixed, the outlet composition ratios of the SOEC stack are determined by π_{ca} and π_{an} based on the mass transport continuity of gases:

$$\begin{cases} P_{H_2O,out} = \frac{(\pi_{ca}-1)}{\pi_{ca}} \cdot \pi_{ca} \\ P_{H_2,in} = P_{H_2,in} + \frac{1}{\pi_{ca}} P_{H_2,in} \\ P_{O_2,out} = \frac{(\pi_{an}+1)P_{O_2,in}}{\pi_{an}+P_{O_2,in}} \\ P_{N_2,out} = \frac{\pi_{an}P_{N_2,in}}{\pi_{an}+P_{N_2,in}} \end{cases} \tag{65}$$

5.1.2.2 Flow Rates

With the inlet composition fixed, the inlet flowrates of different reactants are determined by the cell number n_c, I, $P_{in} = \left[P_{H_2O,in}, P_{H_2,in}, P_{O_2,in}, P_{N_2,in}\right]^T$, π_{ca} and π_{an}:

$$\begin{cases} w_{H_2O,in} = \frac{n_c I}{2F} \cdot \pi_{ca} \\ w_{H_2,in} = w_{H_2O,in} \cdot \frac{P_{H_2,in}}{P_{H_2O,in}} \\ w_{O_2,in} = \frac{n_c I}{4F} \cdot \pi_{an} \\ w_{N_2,in} = w_{O_2,in} \cdot \frac{P_{N_2,in}}{P_{O_2,in}} \end{cases} \tag{66}$$

Similarly, the outlet flowrates of different reactants can also be determined:

$$\begin{cases} w_{H_2O,out} = \frac{n_c I}{2F} \cdot \pi_{ca} \\ w_{H_2,out} = w_{H_2O,out} \cdot \frac{P_{H_2,out}}{P_{H_2O,out}} \\ w_{O_2,out} = \frac{n_c I}{4F} \cdot \pi_{an} \\ w_{N_2,out} = w_{O_2,out} \cdot \frac{P_{N_2,in}}{P_{O_2,in}} \end{cases} \tag{67}$$

5.1.3 Thermal Dynamics

This submodule outputs the dynamic behavior of average stack temperature $\bar{T}$ and the inlet stream temperature T_{in} based on the SOEC thermal dynamics and preheater thermal dynamics, respectively.

5.1.3.1 Solid-Oxide Electrolysis Cell Thermal Dynamics

The thermal energy balance of the SOEC stack can be described as:

$$c_{p,SOEC} \frac{d\bar{T}}{dt} = n_c VI - P_{rea}(T_{out}) - P_{war}(T_{in}, T_{out}, w_{in}) + P_{heat} \tag{68}$$

Where $c_{p,SOEC}$ is the equivalent heat capacity of the SOEC stack, and P_{heat} represents the SOEC stack heater power, P_{war} represents the power used for gas stream warming, P_{rea} corresponds to electrolysis reaction power.

5.1.3.2 Electrolysis Reaction Power

The electrolysis reaction power P_{rea} is related to the enthalpy change of the reaction $\Delta H_R(T)$. Assuming that the inlet and outlet stream temperatures are T_{in} and T_{out}, respectively. P_{rea} can be expressed as:

$$\begin{cases} P_{rea}(T_{out}) = n_c I V_{th} = n_c I \cdot \frac{\Delta H_R(T_{out})}{2F} \approx n_c I \cdot \frac{\Delta H_R(k_T \bar{T})}{2F} \\ \Delta H_R(T) = 238200 - 13.12 \cdot T - 3.55 \cdot 10^{-3} \cdot T^2 \end{cases} \tag{69}$$

In fact, T_{out} is strongly correlated with $\bar{T}$ in a practical condition with constrained stack temperatures and temperature gradients such that T_{out} can be approximately evaluated by:

$$T_{out} \approx k_T \bar{T} \tag{70}$$

Where k_T is a constant that is slightly greater than 1, as estimated by measurement.

5.1.3.3 Steam Warming Power

The gas steam warming power P_{war} is related to the enthalpy increase due to stream warming, and it can be formulated with heat capabilities and temperature increments:

$$P_{war} = (T_{out} - T_{in})\left(c_{p,H_2O} \cdot w_{H_2O,in} + c_{p,H_2} \cdot w_{H_2,in}\right) + (T_{out} - T_{in})\left(c_{p,O_2} \cdot w_{O_2,in} + c_{p,N_2} \cdot w_{N_2,in}\right) \tag{71}$$

Where $c_{p,gas}$ represent the specific capability of different gases.

5.1.3.4 Preheater Thermal Dynamics

The thermal energy balance of the preheater can be described as:

$$c_{p,pre}\frac{dT_{in}}{dt} = P_{heat,pre}(T_{in}, T_{steam}, T_{amb}, w_{in}) + \epsilon_{rec}P_{war,pre} \tag{72}$$

Where $c_{P,pre}$ is the equivalent heat capacity of the preheater, and $P_{heat,pre}$ represents the trim heater power, $P_{war,pre}$ represents the power used for gas stream warming, $\epsilon_{rec}P_{war,pre}$ correspond to the thermal power recycled from the SOEC outlet streams in the fuel heat exchangers, and $\epsilon_{rec} \in (0,1)$ are the effectiveness of the heat exchangers selected through parametric study.

5.2 Hydrogen Electrolysis Dynamical System Scaling

The content shown for this section will be a detailed description of the process to achieve the doubly accelerated current conserved system based on previously run data.

5.2.1 Non-Dimensionalization of Thermal Energy Distribution System Conservation Laws

Similar to Section 4.2.1, the conducted research determined the following steps to complete the data projection: (1) non-dimensionalize the parameters of interest, (2) determine scaling ratios by considering the law of scaling ratios, (3) commence coordinate transformations selection process, and (4) determine projected data based on assumptions, adaptions, and facility restrictions. Expressions for the parameters of interest scaling ratios are shown in Equation (72):

Stack Voltage:
$$\lambda_{A,V} = \frac{V_M^+}{V_P^+}, \quad \lambda_{B,V} = \frac{\left.\frac{\partial V^+}{\partial t}\right|_M}{\left.\frac{\partial V^+}{\partial t}\right|_P}$$

Average Stack Temperature:
$$\lambda_{A,\bar{T}} = \frac{\bar{T}_M^+}{\bar{T}_P^+}, \quad \lambda_{B,\bar{T}} = \frac{\left.\frac{\partial \bar{T}^+}{\partial t}\right|_M}{\left.\frac{\partial \bar{T}^+}{\partial t}\right|_P}$$

Inlet Temperature:
$$\lambda_{A,T_{\text{in}}} = \frac{T_{\text{in,M}}^+}{T_{\text{in,P}}^+}, \quad \lambda_{B,T_{\text{in}}} = \frac{\left.\frac{\partial T_{\text{in}}^+}{\partial t}\right|_M}{\left.\frac{\partial T_{\text{in}}^+}{\partial t}\right|_P} \tag{73}$$

Enthalpy Difference:
$$\lambda_{A,\Delta H} = \frac{\Delta H_M^+}{\Delta H_P^+}, \quad \lambda_{B,\Delta H} = \frac{\left.\frac{\partial \Delta H^+}{\partial t}\right|_M}{\left.\frac{\partial \Delta H^+}{\partial t}\right|_P}$$

In-Out Temperature Difference:
$$\lambda_{A,\theta} = \frac{\theta_M^+}{\theta_P^+}, \quad \lambda_{B,th} = \frac{\left.\frac{\partial \theta^+}{\partial t}\right|_M}{\left.\frac{\partial \theta^+}{\partial t}\right|_P}$$

Inlet and Steam Temperature Difference:

$$\lambda_{A,\theta_{\text{steam}}} = \frac{\theta^+_{\text{steam,M}}}{\theta^+_{\text{steam},P}}, \quad \lambda_{B,\theta_{\text{steam}}} = \frac{\left.\frac{\partial \theta^+_{\text{steam}}}{\partial t}\right|_M}{\left.\frac{\partial \theta^+_{\text{steam}}}{\partial t}\right|_P}$$

Inlet and Ambient Temperature Difference:

$$\lambda_{A,\theta_{\text{amb}}} = \frac{\theta^+_{\text{amb,M}}}{\theta^+_{\text{amb},P}}, \quad \lambda_{B,\theta_{\text{amb}}} = \frac{\left.\frac{\partial \theta^+_{\text{amb}}}{\partial t}\right|_M}{\left.\frac{\partial \theta^+_{\text{amb}}}{\partial t}\right|_P}$$

Stack Heater:

$$\lambda_{A,P_{\text{heat}}} = \frac{P^+_{\text{heat,M}}}{P^+_{\text{heat,P}}}, \quad \lambda_{B,P_{\text{heat}}} = \frac{\left.\frac{\partial P^+_{\text{heat}}}{\partial t}\right|_M}{\left.\frac{\partial P^+_{\text{heat}}}{\partial t}\right|_P}$$

Trim Heater:

$$\lambda_{A,P_{\text{heat,pre}}} = \frac{P^+_{\text{heat,pre,M}}}{P^+_{\text{heat,pre,P}}}, \quad \lambda_{B,P_{\text{heat}}} = \frac{\left.\frac{\partial P^+_{\text{heat,pre}}}{\partial t}\right|_M}{\left.\frac{\partial P^+_{\text{heat,pre}}}{\partial t}\right|_P}$$

5.2.2 Electrical Dynamics and Fluid Dynamics

The differential stack voltage is represented in Equation (56):

$$\frac{\partial V}{\partial t}(I,\bar{T},\bar{P}) = \frac{\partial V_{\text{rev}}}{\partial t}(\bar{T},\bar{P}) + \frac{\partial V_{\text{ohm}}}{\partial t}(I,\bar{T}) + \frac{\partial V_{\text{act}}}{\partial t}(I,\bar{T}) \cdot \frac{1}{1+s\tau_{\text{act}}} + V_{\text{act}}(I,\bar{T}) \cdot \left(\frac{-s}{(1+s\tau_{\text{act}})^2}\frac{\partial \tau_{\text{act}}}{\partial t}\right) \tag{74}$$

From the differential form in Equation (73):

$$V_0 \frac{\partial V^+}{\partial t} = V_{\text{rev},0}\frac{\partial V^+_{\text{rev}}}{\partial t} + V_{\text{ohm},0}\frac{\partial V^+_{\text{ohm}}}{\partial t} + V_{\text{act},0}\frac{\partial V^+_{\text{act}}}{\partial t} \cdot \frac{1}{1+s\tau_{\text{act}}} + V_{\text{act},0}V^+_{\text{act}} \cdot \left(\frac{-s}{(1+s\tau_{\text{act}})^2}\frac{\partial \tau_{\text{act}}}{\partial t}\right) \tag{75}$$

As will be shown in later sections, the SOEC fluid dynamics physics are embedded in the electric dynamics, hence the header for this section. Each of the terms will be non-dimensionalized in the following sections.

5.2.2.1 Reversible Overvoltage

The differential form of Equation (57) is the following:

$$\begin{aligned}\frac{\partial V_{\text{rev}}}{\partial t} = \quad & \frac{\partial V_{\text{oc}}}{\partial t}(\bar{T}) + \frac{\partial \bar{T}}{\partial t}\frac{R}{2F}\ln\left(\frac{\bar{P}_{\text{H}_2}\bar{P}^{0.5}_{\text{O}_2}}{\bar{P}_{\text{H}_2\text{O}}}\right) \\ & + \frac{R\bar{T}}{2F}\frac{\bar{P}_{\text{H}_2\text{O}}}{\bar{P}_{\text{H}_2}\bar{P}^{0.5}_{\text{O}_2}}\left[\left(\frac{1}{\bar{P}^2_{\text{H}_2\text{O}}}\right)\left(\frac{\partial \bar{P}_{\text{H}_2}}{\partial t}\bar{P}^{0.5}_{\text{O}_2}\bar{P}_{H_2O} + \frac{\bar{P}_{\text{H}_2}}{2}\left\{\frac{\partial \bar{P}_{\text{O}_2}}{\partial t}\right\}^{-0.5}\bar{P}_{\text{H}_2\text{O}} - \bar{P}_{\text{H}_2}\bar{P}_{\text{O}_2}\frac{\partial \bar{P}_{\text{H}_2\text{O}}}{\partial t}\right)\right]\end{aligned} \tag{76}$$

Plugging in terms and considering the associated voltage of Gibbs Free Energy of the reaction:

$$\begin{aligned}\frac{\partial V_{\text{rev}}}{\partial t} = \quad & \frac{-49.18 - 5.44 \cdot 10^{-3} \cdot \bar{T}}{2F}\frac{\partial \bar{T}}{\partial t} + \frac{R}{2F}\ln\left(\frac{\bar{P}_{\text{H}_2}\bar{P}_{\text{O}_2}^{0.5}}{\bar{P}_{\text{H}_2\text{O}}}\right)\frac{\partial \bar{T}}{\partial t} \\ & + \frac{R\bar{T}}{2F}\frac{1}{\bar{P}_{\text{H}_2}\bar{P}_{\text{O}_2}^{0.5}\bar{P}_{\text{H}_2\text{O}}}\left[\bar{P}_{\text{O}_2}^{0.5}\bar{P}_{H_2O}\frac{\partial \bar{P}_{\text{H}_2}}{\partial t} + \frac{\bar{P}_{\text{H}_2}\bar{P}_{\text{H}_2\text{O}}}{2}\left\{\frac{\partial \bar{P}_{\text{O}_2}}{\partial t}\right\}^{-0.5} - \bar{P}_{\text{H}_2}\bar{P}_{\text{O}_2}\frac{\partial \bar{P}_{\text{H}_2\text{O}}}{\partial t}\right]\end{aligned} \tag{77}$$

Consider the partial pressures in Equations (62), (63), and (64):

$$\frac{\partial V_{\text{rev}}}{\partial t} = \quad \frac{-49.18 - 5.44 \cdot 10^{-3} \cdot \bar{T}}{2F}\frac{\partial \bar{T}}{\partial t} + \frac{R}{2F}\ln\left(\frac{\bar{P}_{\text{H}_2}\bar{P}_{\text{O}_2}^{0.5}}{\bar{P}_{\text{H}_2\text{O}}}\right)\frac{\partial \bar{T}}{\partial t} + \frac{R\bar{T}}{2F}\frac{1}{\bar{P}_{\text{H}_2}\bar{P}_{\text{O}_2}^{0.5}\bar{P}_{\text{H}_2\text{O}}}[A + B - C] \tag{78}$$

Where A, B, and C are shown in Equation (78):

$$\begin{aligned}A\text{:} \quad & \frac{P_{\text{H}_2,\text{in}}^{(1-\lambda)}P_{\text{H}_2,\text{out}}^{\lambda}\bar{P}_{\text{O}_2}^{0.5}\bar{P}_{H_2O}}{1 + s\tau_{\text{H}_2}}\left\{(1-\lambda)P_{\text{H}_2,\text{in}}^{-1}\frac{\partial P_{\text{H}_2,\text{in}}}{\partial t} + \lambda P_{\text{H}_2,\text{out}}^{-1}\frac{\partial P_{\text{H}_2,\text{out}}}{\partial t} + \left(\frac{-s}{1 + s\tau_{\text{H}_2}}\frac{\partial \tau_{\text{H}_2}}{\partial t}\right)\right\} \\ B\text{:} \quad & \frac{\bar{P}_{\text{H}_2}P_{\text{O}_2,\text{in}}^{-0.5(1-\lambda)}P_{\text{O}_2,\text{out}}^{-0.5\lambda}\bar{P}_{\text{H}_2\text{O}}}{2\left(1 + s\tau_{\text{O}_2}\right)^{-0.5}}\left\{(1-\lambda)P_{\text{O}_2,\text{in}}^{-1}\frac{\partial P_{\text{O}_2,\text{in}}}{\partial t} + \lambda P_{\text{O}_2,\text{out}}^{-1}\frac{\partial P_{\text{O}_2,\text{out}}}{\partial t} \right. \\ & \left. + \left(\frac{-s}{1 + s\tau_{\text{O}_2}}\frac{\partial \tau_{\text{O}_2}}{\partial t}\right)\right\}^{-0.5} \\ C\text{:} \quad & \frac{\bar{P}_{\text{H}_2}\bar{P}_{\text{O}_2}P_{\text{H}_2\text{O},\text{in}}^{(1-\lambda)}P_{\text{H}_2\text{O},\text{out}}^{\lambda}}{1 + s\tau_{\text{H}_2\text{O}}}\left\{(1-\lambda)P_{\text{H}_2\text{O},\text{in}}^{-1}\frac{\partial P_{\text{H}_2\text{O},\text{in}}}{\partial t} + \lambda P_{\text{H}_2\text{O},\text{out}}^{-1}\frac{\partial P_{\text{H}_2\text{O},\text{out}}}{\partial t} \right. \\ & \left. + \left(\frac{-s}{1 + s\tau_{\text{H}_2\text{O}}}\frac{\partial \tau_{\text{H}_2\text{O}}}{\partial t}\right)\right\}\end{aligned} \tag{79}$$

The current (by adjusting applied voltage) and supply of species are kept constant. Feed factors are constant as well:

$$\begin{aligned}A\text{:} \quad & P_{\text{H}_2,\text{in}}^{-1}\frac{\partial P_{\text{H}_2,\text{in}}}{\partial t} + \left(\frac{-s}{1 + s\tau_{\text{H}_2}}\frac{\partial \tau_{\text{H}_2}}{\partial t}\right) \\ B\text{:} \quad & \frac{1}{2}\left\{\frac{(1-\lambda)\left(\pi_{\text{an}} + P_{\text{O}_2,\text{in}}\right) + \lambda\left(1 - P_{\text{O}_2,\text{in}}\right)}{\left(\pi_{\text{an}} + P_{\text{O}_2,\text{in}}\right)P_{\text{O}_2,\text{in}}}\frac{\partial P_{\text{O}_2,\text{in}}}{\partial t} + \left(\frac{-s}{1 + s\tau_{\text{O}_2}}\frac{\partial \tau_{\text{O}_2}}{\partial t}\right)\right\}^{-0.5} \\ C\text{:} \quad & P_{\text{H}_2\text{O},\text{in}}^{-1}\frac{\partial P_{\text{H}_2\text{O},\text{in}}}{\partial t} + \left(\frac{-s}{1 + s\tau_{\text{H}_2\text{O}}}\frac{\partial \tau_{\text{H}_2\text{O}}}{\partial t}\right)\end{aligned} \tag{80}$$

Replace outlet pressure with inlet pressure and consider $\xi_{\mathrm{H_2}} = 1 + s\tau_{\mathrm{H_2}}$, $\xi_{\mathrm{O_2}} = 1 + s\tau_{\mathrm{O_2}}$, and $\xi_{\mathrm{H_2O}} = 1 + s\tau_{\mathrm{H_2O}}$:

$$
\begin{aligned}
&A: \quad P_{\mathrm{H_2,in}}^{-1}\frac{\partial P_{\mathrm{H_2,in}}}{\partial t} + \left(\frac{-1}{\xi_{\mathrm{H_2}}}\frac{\partial \xi_{\mathrm{H_2}}}{\partial t}\right)\\
&B: \quad \frac{1}{2}\left\{\frac{(1-\lambda)\left(\pi_{\mathrm{an}} + P_{\mathrm{O_2,in}}\right) + \lambda\left(1 - P_{\mathrm{O_2,in}}\right)}{\left(\pi_{\mathrm{an}} + P_{\mathrm{O_2,in}}\right)P_{\mathrm{O_2,in}}}\frac{\partial P_{\mathrm{O_2,in}}}{\partial t} + \left(\frac{-1}{\xi_{\mathrm{O_2}}}\frac{\partial \xi_{\mathrm{O_2}}}{\partial t}\right)\right\}^{-0.5}\\
&C: \quad P_{\mathrm{H_2O,in}}^{-1}\frac{\partial P_{\mathrm{H_2O,in}}}{\partial t} + \left(\frac{-1}{\xi_{\mathrm{H_2O}}}\frac{\partial \xi_{H_2O}}{\partial t}\right)
\end{aligned}
\tag{81}
$$

The non-dimensionalized equation is then:

$$
\begin{aligned}
V_{\mathrm{rev},0}\frac{\partial V_{\mathrm{rev}}^{+}}{\partial t} = \quad & \frac{-49.18\bar{T}_0 - 5.44\cdot 10^{-3}\cdot \bar{T}_0^2}{2F}\frac{\partial \bar{T}^{+}}{\partial t}\\
& + \frac{R\bar{T}_0}{2F}\ln\left(\frac{\left[\left(\frac{\pi_{\mathrm{ca}}+1}{\pi_{\mathrm{ca}}}\right)^{\lambda}\frac{1}{1+s\tau_{\mathrm{H_2}}}\right]\left[\left(\frac{\pi_{\mathrm{an}}+1}{\pi_{\mathrm{an}}+P_{\mathrm{O_2,in}}}\right)^{\lambda}\frac{1}{1+s\tau_{\mathrm{O_2}}}\right]}{\left[\left(\frac{\pi_{\mathrm{ca}}-1}{\pi_{\mathrm{ca}}}\right)^{\lambda}\frac{1}{1+s\tau_{\mathrm{H_2O}}}\right]}\right)\frac{\partial \bar{T}^{+}}{\partial t}\\
& + \frac{R\bar{T}_0\bar{T}^{+}}{2F}[A + B - C]
\end{aligned}
\tag{82}
$$

$$
\begin{aligned}
&A: \quad \frac{1}{P_{\mathrm{H_2,in}}^{+}}\frac{\partial P_{\mathrm{H_2,in}}^{+}}{\partial t} + \left(\frac{-1}{\xi_{H_2}^{+}}\frac{\partial \xi_{H_2}^{+}}{\partial t}\right)\\
&B: \quad \frac{1}{2}\left\{\frac{(1-\lambda)\left(\pi_{\mathrm{an}} + P_{\mathrm{O_2,in,0}}P_{\mathrm{O_2,in}}^{+}\right) + \lambda\left(1 - P_{\mathrm{O_2,in,0}}P_{\mathrm{O_2,in}}^{+}\right)}{\left(\pi_{\mathrm{an}} + P_{\mathrm{O_2,in,0}}P_{\mathrm{O_2,in}}^{+}\right)P_{\mathrm{O_2,in}}^{+}}\frac{\partial P_{\mathrm{O_2,in}}^{+}}{\partial t} + \left(\frac{-1}{\xi_{\mathrm{O_2}}^{+}}\frac{\partial \xi_{\mathrm{O_2}}^{+}}{\partial t}\right)\right\}^{-0.5}\\
&C: \quad \frac{1}{P_{\mathrm{H_2O,in}}^{+}}\frac{\partial P_{\mathrm{H_2O,in}}^{+}}{\partial t} + \left(\frac{-1}{\xi_{\mathrm{H_2O}}^{+}}\frac{\partial \xi_{\mathrm{H_2O}}^{+}}{\partial t}\right)
\end{aligned}
$$

The differential temperature first-order delay effects scaling ratio based on the law of scaling ratios is:

$$
\lambda_{B,V} = \left(\ln\left(\frac{\left[\left(\frac{\pi_{\mathrm{ca}}+1}{\pi_{\mathrm{ca}}}\right)^{\lambda}\frac{1}{1+s\tau_{\mathrm{H_2}}}\right]\left[\left(\frac{\pi_{\mathrm{an}}+1}{\pi_{\mathrm{an}}+P_{\mathrm{O_2,in}}}\right)^{\lambda}\frac{1}{1+s\tau_{\mathrm{O_2}}}\right]}{\left[\left(\frac{\pi_{\mathrm{ca}}-1}{\pi_{\mathrm{ca}}}\right)^{\lambda}\frac{1}{1+s\tau_{\mathrm{H_2O}}}\right]}\right)^{\frac{\bar{T}_0}{V_0}}\right)_R \lambda_{B,\bar{T}} \tag{83}
$$

The hydrogen differential pressure first-order delay effects scaling ratio is:

$$
\lambda_{A,V} = \left(\frac{\bar{T}_0}{V_0}\right)_R \lambda_{A,\bar{T}} \tag{84}
$$

5.2.2.2 Ohmic Overvoltage

The differential form of Equation (59) is the following:

$$
\frac{\partial V_{\mathrm{ohm}}}{\partial t} = \frac{\partial I}{\partial t}\cdot A \cdot ASR(\bar{T}) + I\cdot\frac{\partial A}{\partial t}\cdot ASR(\bar{T}) + I\cdot A\cdot\frac{\partial ASR}{\partial t}(\bar{T}) \tag{85}
$$

Plugging in terms and considering area-specific resistance:

$$\frac{\partial V_{\text{ohm}}}{\partial t} = \frac{\partial I}{\partial t} \cdot A \cdot \left(ASR(T_{\text{ref}}) - 0.463 + 3.973 \cdot 10^{-5} \cdot e^{\frac{10300}{\bar{T}}} \right) + I \cdot \frac{\partial A}{\partial t} \cdot \left(ASR(T_{\text{ref}}) - 0.463 + 3.973 \cdot 10^{-5} \cdot e^{\frac{10300}{\bar{T}}} \right) + I \cdot A \cdot \left(\frac{\partial ASR}{\partial t}(T_{\text{ref}}) - \frac{0.409219}{\bar{T}} \frac{\partial \bar{T}}{\partial t} \cdot e^{\frac{10300}{\bar{T}}} \right) \tag{86}$$

Cell area is time independent:

$$\frac{\partial V_{\text{ohm}}}{\partial t} = \frac{\partial I}{\partial t} \cdot A \cdot \left(ASR(T_{\text{ref}}) - 0.463 + 3.973 \cdot 10^{-5} \cdot e^{\frac{10300}{\bar{T}}} \right) - I \cdot A \cdot \left(\frac{0.409219}{\bar{T}} \frac{\partial \bar{T}}{\partial t} \cdot e^{\frac{10300}{\bar{T}}} \right) \tag{87}$$

Keep current as constant as possible to satisfy a steady generation of hydrogen:

$$\frac{\partial V_{\text{ohm}}}{\partial t} = I \cdot A \cdot \left(\frac{0.409219}{\bar{T}} \frac{\partial \bar{T}}{\partial t} \cdot e^{\frac{10300}{\bar{T}}} \right) \tag{88}$$

The non-dimensionalized equation is then:

$$V_{\text{ohm},0} \frac{\partial V_{\text{ohm}}^{+}}{\partial t} = IA \left(\frac{0.409219}{\bar{T}^{+}} \frac{\partial \bar{T}^{+}}{\partial t} e^{\frac{10300}{\bar{T}}} \right) \tag{89}$$

The ohmic effect scaling ratio based on law of scaling ratios is:

$$\lambda_{A,V} = \left(\frac{IA\bar{T}_0 e^{\frac{10300}{\bar{T}}}}{V_0} \right)_R \tag{90}$$

5.2.2.3 Activation Overvoltage

The differential form of Equation (61) is the following:

$$\frac{\partial V_{\text{act}}}{\partial t} = \frac{\partial \bar{T}}{\partial t} \frac{R}{2F} \left[\sinh^{-1}\left(\frac{I}{2I_{\text{ex,ca}}} \right) + \sinh^{-1}\left(\frac{I}{2I_{\text{ex,an}}} \right) \right] + \frac{R\bar{T}}{2F} \left[\frac{1}{\sqrt{\left(\frac{I}{2I_{\text{ex,ca}}} \right)^2 + 1}} \frac{\partial}{\partial t}\left(\frac{I}{2I_{\text{ex,ca}}} \right) + \frac{1}{\sqrt{\left(\frac{I}{2I_{\text{ex,an}}} \right)^2 + 1}} \frac{\partial}{\partial t}\left(\frac{I}{2I_{\text{ex,an}}} \right) \right] \tag{91}$$

Apply constant current (as mentioned in Section 5.1.1.2) and time dependent exchange current:

$$\frac{\partial V_{\text{act}}}{\partial t} = \frac{\partial \bar{T}}{\partial t} \frac{R}{2F} \left[\sinh^{-1}\left(\frac{I}{2I_{\text{ex,ca}}} \right) + \sinh^{-1}\left(\frac{I}{2I_{\text{ex,an}}} \right) \right] - \frac{R\bar{T}}{2F} \left[\frac{1}{\sqrt{\left(\frac{I}{2I_{\text{ex,ca}}} \right)^2 + 1}} \frac{I}{2I_{\text{ex,ca}}^2} \frac{\partial I_{\text{ex,ca}}}{\partial t} + \frac{1}{\sqrt{\left(\frac{I}{2I_{\text{ex,an}}} \right)^2 + 1}} \frac{I}{2I_{\text{ex,an}}^2} \frac{\partial I_{\text{ex,an}}}{\partial t} \right] \tag{92}$$

Plug in exchange current and assume the pre-exponential factor and activation energy is reaction dependent and weakly temperature dependent:

$$\frac{\partial V_{\text{act}}}{\partial t} = \frac{\partial \bar{T}}{\partial t}\frac{R}{2F}\left[\sinh^{-1}\left(\frac{I}{2I_{\text{ex,ca}}}\right) + \sinh^{-1}\left(\frac{I}{2I_{\text{ex,an}}}\right)\right.$$
$$- \frac{IR\bar{T}}{4FI_{\text{ex,ca}}^2\sqrt{\left(\frac{I}{2I_{\text{ex,ca}}}\right)^2+1}}\left(1 - \Gamma_{\text{ex,ca}}\frac{2\xi_{\text{ca}}}{R\bar{T}}e^{-\frac{\xi_{\text{ca}}}{R\bar{T}}}\right) \tag{93}$$
$$\left. - \frac{IR\bar{T}}{4FI_{\text{ex,an}}^2\sqrt{\left(\frac{I}{2I_{\text{ex,an}}}\right)^2+1}}\left(1 - \Gamma_{\text{ex,an}}\frac{2\xi_{\text{an}}}{R\bar{T}}e^{-\frac{\xi_{\text{an}}}{R\bar{T}}}\right)\right]$$

The non-dimensionalized equation is then:

$$V_{\text{act}}\frac{\partial V_{\text{act}}^{+}}{\partial t} = \frac{\bar{T}_0 R}{2F}\frac{\partial \bar{T}^{+}}{\partial t}\left[\sinh^{-1}\left(\frac{I}{2I_{\text{ex,ca}}}\right) + \sinh^{-1}\left(\frac{I}{2I_{\text{ex,an}}}\right)\right.$$
$$- \frac{I}{4FI_{\text{ex,ca}}^2\sqrt{\left(\frac{I}{2I_{\text{ex,ca}}}\right)^2+1}}\left(\bar{T}_0\bar{T}^{+} - 2\Gamma_{\text{ex,ca}}\xi_{\text{ca}}e^{-\frac{\xi_{\text{ca}}}{R\bar{T}}}\right) \tag{94}$$
$$\left. - \frac{I}{4FI_{\text{ex,an}}^2\sqrt{\left(\frac{I}{2I_{\text{ex,an}}}\right)^2+1}}\left(\bar{T}_0\bar{T}^{+} - 2\Gamma_{\text{ex,an}}\xi_{\text{an}}e^{-\frac{\xi_{\text{an}}}{R\bar{T}}}\right)\right]$$

The cathode differential temperature effect scaling ratio based on law of scaling ratios is:

$$\lambda_{B,V} = \left[\frac{\bar{T}_0}{V_0}\sinh^{-1}\left(\frac{I}{2I_{\text{ex,ca}}}\right)\right]_R \lambda_{B,\bar{T}} \tag{95}$$

The cathode temperature effect scaling ratio based on law of scaling ratios is:

$$\lambda_{B,V} = \left[\frac{I\bar{T}_0}{V_0 I_{\text{ex,ca}}^2\sqrt{\left(\frac{I}{2I_{\text{ex,ca}}}\right)^2+1}}\right]_R \lambda_{A,\bar{T}}\lambda_{B,\bar{T}} \tag{96}$$

The anode differential temperature effect scaling ratio based on law of scaling ratios is:

$$\lambda_{B,V} = \left[\frac{\bar{T}_0}{V_0}\sinh^{-1}\left(\frac{I}{2I_{\text{ex,an}}}\right)\right]_R \lambda_{B,\bar{T}} \tag{97}$$

The anode temperature effect scaling ratio based on law of scaling ratios is:

$$\lambda_{B,V} = \left[\frac{I\bar{T}_0}{V_0 I_{\text{ex,an}}^2\sqrt{\left(\frac{I}{2I_{\text{ex,an}}}\right)^2+1}}\right]_R \lambda_{A,\bar{T}}\lambda_{B,\bar{T}} \tag{98}$$

5.2.3 Thermal Dynamics

The thermal dynamics are divided into two sections: (1) SOEC thermal dynamics and (2) preheater thermal dynamics. Together, both will characterize the full high-temperature hydrogen electrolysis thermal dynamics and will be scaled separately.

5.2.3.1 Solid-Oxide Electrolysis Cell Thermal Dynamics

Non-dimensionalize the average stack temperature from Equation (67) by a certain reference value:

$$\frac{d\bar{T}^+}{dt} = \frac{n_c V I}{\bar{T}_0 C_{\text{SOEC}}} - \frac{P_{\text{rea}}(T_{\text{out}})}{\bar{T}_0 C_{\text{SOEC}}} - \frac{P_{\text{war}}(T_{\text{in}},T_{\text{out}},w_{\text{in}})}{\bar{T}_0 C_{\text{SOEC}}} + \frac{P_{\text{heat}}}{\bar{T}_0 C_{\text{SOEC}}}\lambda_{B,V} \tag{99}$$

To consider electrolysis reaction power and steam warming power, plug in Equations (68) and (70):

$$\begin{aligned}\frac{d\bar{T}^+}{dt} = \quad & \frac{n_c V I}{\bar{T}_0 C_{\text{SOEC}}} - \frac{n_c I \Delta H_R(k_T\bar{T})}{2F\bar{T}_0 C_{\text{SOEC}}} + \frac{P_{\text{heat}}}{\bar{T}_0 C_{\text{SOEC}}} \\ & - \frac{T_{\text{out}} - T_{\text{in}}}{4F\bar{T}_0 C_{\text{SOEC}}}\left\{2c_{p,\text{H}_2\text{O}} n_c I\pi_{\text{ca}} + \frac{2c_{P,\text{H}_2} n_c I\pi_{\text{ca}} P_{\text{H}_2,\text{in}}}{P_{\text{H}_2\text{O,in}}} + c_{\text{P,O}_2} n_c I\pi_{\text{an}}\right. \\ & \left. + \frac{c_{\text{P},N_2} n_c I\pi_{\text{an}} P_{\text{N}_2,\text{in}}}{P_{\text{O}_2,\text{in}}}\right\}\end{aligned} \tag{100}$$

From Equation (99), non-dimensionalize the SOEC thermal dynamics:

$$\begin{aligned}\frac{d\bar{T}^+}{dt} = \quad & \frac{n_c V_0 V^+ I}{\bar{T}_0 c_{\text{P,SOEC}}} - \frac{n_c I \Delta H_0 \Delta H_R^+}{2F\bar{T}_0 c_{\text{P,SOEC}}} + \frac{P_{\text{heat},0} P_{\text{heat}}^+}{\bar{T}_0 c_{\text{P,SOEC}}} \\ & - \frac{\theta_0\theta^+}{4F\bar{T}_0 c_{\text{P,SOEC}}}\left\{2c_{\text{P,H}_2\text{O}} n_c I\pi_{\text{ca}} + \frac{2c_{\text{P,H}_2} n_c I\pi_{\text{ca}} P_{\text{H}_2,\text{in},0} P_{\text{H}_2,\text{in}}^+}{P_{\text{H}_2\text{O,in},0} P_{\text{H}_2\text{O,in}}^+} + c_{\text{P,O}_2} n_c I\pi_{\text{an}}\right. \\ & \left. + \frac{c_{\text{P},N_2} n_c I\pi_{\text{an}} P_{\text{N}_2,\text{in},0} P_{\text{N}_2,\text{in}}^+}{P_{\text{O}_2,\text{in},0} P_{\text{O}_2,\text{in}}^+}\right\}\end{aligned} \tag{101}$$

The differential temperature ratio in terms of voltage and specific heat based on law of scaling ratios is:

$$\lambda_{B,T} = \left(\frac{n_c V_0 I}{\bar{T}_0 c_{\text{P,SOEC}}}\right)_R \lambda_{A,V} \tag{102}$$

The differential temperature ratio in terms of enthalpy change based on law of scaling ratios is:

$$\lambda_{B,T} = \left(\frac{n_c I \Delta H_0}{\bar{T}_0 c_{\text{P,SOEC}}}\right)_R \lambda_{A,\Delta H} \tag{103}$$

The differential temperature ratio in terms of stack heater based on law of scaling ratios is:

$$\lambda_{B,T} = \left(\frac{P_{\text{heat},0}}{\bar{T}_0 c_{\text{P,SOEC}}}\right)_R \lambda_{A,P_{\text{heat}}} \tag{104}$$

The differential temperature ratio in terms of differential hydrogen pressure based on law of scaling ratios is:

$$\lambda_{B,T} = \left(\frac{c_{\text{P,H}_2} n_c I \pi_{\text{ca}} P_{\text{H}_2,\text{in},0} \theta_0}{\bar{T}_0 c_{\text{P,SOEC}} P_{\text{H}_2\text{O,in},0}}\right)_R \lambda_{A,\theta} \tag{105}$$

The differential temperature ratio in terms of water-specific heat temperature difference based on law of scaling ratios is:

$$\lambda_{B,T} = \left(\frac{c_{\text{P,H}_2\text{O}} n_c I \pi_{\text{ca}} \theta_0}{\bar{T}_0 c_{\text{P,SOEC}}}\right)_R \lambda_{A,\theta} \tag{106}$$

The differential temperature ratio in terms of oxygen-specific heat temperature difference based on law of scaling ratios is:

$$\lambda_{B,T} = \left(\frac{c_{\text{P,O}_2} n_c I \pi_{\text{an}} \theta_0}{\bar{T}_0 c_{\text{P,SOEC}}}\right)_R \lambda_{A,\theta} \tag{107}$$

The differential temperature ratio in terms of nitrogen specific heat based on law of scaling ratios is:

$$\lambda_{B,T} = \left(\frac{c_{\text{P},N_2} n_c I \pi_{\text{an}} P_{\text{N}_2,\text{in},0} \theta_0}{\bar{T}_0 c_{\text{P,SOEC}} P_{\text{O}_2,\text{in},0}}\right)_R \lambda_{A,\theta} \tag{108}$$

5.2.3.2 Preheater Thermal Dynamics

Non-dimensionlize the average stack temperature from Equation (71) by a certain reference value:

$$\frac{dT_{\text{in}}^+}{dt} = \frac{P_{\text{heat,pre}}}{c_{\text{P,pre}} T_{\text{in},0}} - \frac{P_{\text{war,pre}}}{c_{\text{P,pre}} T_{\text{in},0}} + \frac{\epsilon_{\text{rec}} P_{\text{war,pre}}}{c_{\text{P,pre}} T_{\text{in},0}} \tag{109}$$

To consider electrolysis reaction power and steam warming power, plug in Equations (68) and (70):

$$\begin{aligned}\frac{dT_{\text{in}^+}}{dt} = \quad & \frac{P_{\text{heat,pre}}}{c_{\text{P,pre}}} + \frac{(1-\epsilon)}{c_{\text{P,pre}}}\left\{\theta_{\text{steam}}\left(\frac{c_{\text{P,H}_2\text{O}} n_c I \pi_{\text{ca}}}{2F} + \frac{c_{\text{P,H}_2} n_c I \pi_{\text{ca}} P_{\text{H}_2,\text{in}}}{2F P_{\text{H}_2\text{O,in}}}\right)\right. \\ & \left. - \theta_{\text{amb}}\left(\frac{c_{\text{P,O}_2} n_c I \pi_{\text{an}}}{4F} + \frac{c_{\text{P,N}_2} n_c I \pi_{\text{an}} P_{\text{N}_2,\text{in}}}{4F P_{\text{O}_2,\text{in}}}\right)\right\}\end{aligned} \tag{110}$$

From Equation (109), non-dimensionalize the preheater thermal dynamics:

$$\begin{aligned}\frac{dT_{\text{in}}^+}{dt} = \quad & \frac{P_{\text{heat,pre},0} P_{\text{heat,pre}}^+}{c_{\text{P,pre}} T_{\text{in},0}} + \\ & \frac{(1-\epsilon)}{c_{\text{P,pre}} T_{\text{in},0}}\left\{\theta_{\text{steam},0}\theta_{\text{steam}}^+\left(\frac{c_{\text{P,H}_2\text{O}} n_c I \pi_{\text{ca}}}{2F} + \frac{c_{\text{P,H}_2} n_c I \pi_{\text{ca}} P_{\text{H}_2,\text{in},0} P_{\text{H}_2,\text{in}}^+}{2F P_{\text{H}_2\text{O,in},0} P_{\text{H}_2\text{O,in}}^+}\right)\right. \\ & \left. - \theta_{\text{amb},0}\theta_{\text{amb}}^+\left(\frac{c_{\text{P,O}_2} n_c I \pi_{\text{an}}}{4F} + \frac{c_{\text{P,N}_2} n_c I \pi_{\text{an}} P_{\text{N}_2,\text{in},0} P_{\text{N}_2,\text{in}}^+}{4F P_{\text{O}_2,\text{in},0} P_{\text{O}_2,\text{in}}^+}\right)\right\}\end{aligned} \tag{111}$$

The differential inlet temperature in terms of trim heater power based on law of scaled ratios is:

$$\lambda_{B,T_{\text{in}}} = \left(\frac{P_{\text{heat,pre},0}}{c_{\text{P,pre}} T_{\text{in},0}}\right)_R \lambda_{A,P_{\text{heat,pre}}} \tag{112}$$

The differential inlet temperature in terms of cathode Inlet-steam temperature difference with water-specific heat based on law of scaled ratios is:

$$\lambda_{B,T_{\text{in}}} = \left(\frac{c_{P,\text{H}_2\text{O}} n_c I \pi_{\text{ca}} \theta_{\text{steam},0}(1-\epsilon)}{c_{\text{P,pre}} T_{\text{in},0}}\right)_R \lambda_{A,\theta_{\text{steam}}} \tag{113}$$

The differential inlet temperature in terms of cathode inlet-steam temperature difference with hydrogen-specific heat based on the law of scaled ratios is:

$$\lambda_{B,T_{\text{in}}} = \left(\frac{c_{P,\text{H}_2} n_c I \pi_{\text{ca}} P_{\text{H}_2,\text{in}} \theta_{\text{steam},0}(1-\epsilon)}{c_{\text{P,pre}} T_{\text{in},0} P_{\text{H}_2\text{O,in}}}\right)_R \lambda_{A,\theta_{\text{steam}}} \tag{114}$$

The differential inlet temperature in terms of anode Inlet-ambient temperature difference with oxygen-specific heat based on law of scaled ratios is:

$$\lambda_{B,T_{\text{in}}} = \left(\frac{c_{p,\text{O}_2} n_c I \pi_{\text{an}} \theta_{\text{amp},0}(1-\epsilon)}{c_{\text{P,pre}} T_{\text{in},0}}\right)_R \lambda_{A,\theta_{\text{amp}}} \tag{115}$$

The differential inlet temperature in terms of anode Inlet-ambient temperature difference with nitrogen specific heat based on law of scaled ratios is:

$$\lambda_{B,T_{\text{in}}} = \left(\frac{c_{P,\text{N}_2} n_c I \pi_{\text{an}} P_{\text{H}_2,\text{in}} \theta_{\text{amp},0}(1-\epsilon)}{c_{\text{P,pre}} T_{\text{in},0} P_{\text{H}_2\text{O,in}}}\right)_R \lambda_{A,\theta_{\text{amb}}} \tag{116}$$

5.3 Hydrogen Electrolysis Hierarchal Two-Tiered Scaling

The content shown for this section will be a detailed description of the process to achieve the doubly accelerated current conserved system based on previously run data.

5.3.1 Non-Dimensionalization of Hierarchal Two-Tiered Scaling Conservation Laws

Similar to Section 4.3.1, the following steps are required complete the data projection: (1) non-dimensionalize governing laws, (2) derive residence time and characteristic time ratio for each governing law, (3) determine projected nominal conditions to keep scaled characteristic time ratio groups equivalent to the base case, and (4) balance relations to ensure the projected residence time is half of the base case. The reference point to normalize each parameter is the mode transition time point.

5.3.2 Electrical Dynamics

The following are the relations to normalize each parameter by the selected reference data point:

$$\begin{gathered}
V^+ = \frac{V}{V_0}, \quad V_{\text{rev}}^+ = \frac{V_{\text{rev}}}{V_{\text{rev},0}}, \quad V_{\text{ohm}}^+ = \frac{V_{\text{ohm}}}{\text{V}_{\text{ohm},0}}, \quad V_{\text{act}}^+ = \frac{V_{\text{act}}}{V_{\text{act},0}}, \quad \bar{T}^+ = \frac{\bar{T}}{\bar{T}_0}, \\
P_{\text{H}_2,\text{in}}^+ = \frac{P_{\text{H}_2,\text{in}}}{P_{\text{H}_2,\text{in},0}}, \quad \xi_{\text{H}_2}^+ = \frac{\xi_{\text{H}_2}}{\xi_{\text{H}_2,0}} = \frac{1+s\tau_{\text{H}_2}}{1+s\tau_{\text{H}_2,0}}, \quad P_{\text{O}_2,\text{in}}^+ = \frac{P_{\text{O}_2,\text{in}}}{P_{\text{O}_2,\text{in},0}}, \\
\xi_{\text{O}_2}^+ = \frac{\xi_{\text{O}_2}}{\xi_{\text{O}_2,0}} = \frac{1+s\tau_{\text{O}_2}}{1+s\tau_{\text{O}_2,0}}, \quad P_{\text{H}_2\text{O,in}}^+ = \frac{P_{\text{H}_2\text{O,in}}}{P_{\text{H}_2\text{O,in},0}}, \quad \xi_{\text{H}_2\text{O}}^+ = \frac{\xi_{\text{H}_2\text{O}}}{\xi_{\text{H}_2\text{O},0}} = \frac{1+s\tau_{\text{H}_2\text{O}}}{1+s\tau_{\text{H}_2\text{O},0}}
\end{gathered} \tag{117}$$

From the differential form in Equation (73), normalize and reorganize terms:

$$V_0 \frac{\partial V^+}{\partial t} = V_{\text{rev},0} \frac{\partial V_{\text{rev}}^+}{\partial t} + V_{\text{ohm},0} \frac{\partial V_{\text{ohm}}^+}{\partial t} + V_{\text{act},0} \frac{\partial V_{\text{act}}^+}{\partial t} \cdot \frac{1}{1+s\tau_{\text{act}}} + V_{\text{act},0} V_{\text{act}}^+ \cdot \left(\frac{-s}{(1+s\tau_{\text{act}})^2} \frac{\partial \tau_{\text{act}}}{\partial t}\right) \tag{118}$$

As will be shown in later sections, the SOEC fluid dynamics physics are embedded in the electric dynamics, hence the header for this section. Each of the terms will be non-dimensionalized in the following sections.

5.3.2.1 Reversible Overvoltage

Use Equation (81) from Section 5.2.2.1.

5.3.2.2 Ohmic Overvoltage

Use Equation (88) from Section 5.2.2.2.

5.3.2.3 Activation Overvoltage

Use Equation (93) from Section 5.2.2.3.

5.3.2.4 Overall Stack Voltage Residence Time and Characterized Time Ratio

The overall expression is:

$$\begin{aligned}\frac{V_0 F}{R\bar{T}_0}\frac{\partial V^+}{\partial t} = \quad & \frac{-49.18 - 5.44\cdot 10^{-3}\bar{T}_0}{2R}\frac{\partial \bar{T}^+}{\partial t} \\ & + \frac{1}{2}\ln\left(\frac{\left[\left(\frac{\pi_{\mathrm{ca}}+1}{\pi_{\mathrm{ca}}}\right)^{\lambda}\frac{1}{1+s\tau_{\mathrm{H_2}}}\right]\left[\left(\frac{\pi_{\mathrm{an}}+1}{\pi_{\mathrm{an}}+P_{\mathrm{O_2,in}}}\right)^{\lambda}\frac{1}{1+s\tau_{\mathrm{O_2}}}\right]}{\left[\left(\frac{\pi_{\mathrm{ca}}-1}{\pi_{\mathrm{ca}}}\right)^{\lambda}\frac{1}{1+s\tau_{\mathrm{H_2O}}}\right]}\right)\frac{\partial \bar{T}^+}{\partial t} \\ & + \frac{\bar{T}^+}{2}[A+B-C] \\ & + \frac{IAF}{R\bar{T}_0}\left(\frac{0.409219}{\bar{T}^+}\frac{\partial \bar{T}^+}{\partial t}e^{\frac{10300}{\bar{T}_0\bar{T}^+}}\right) \\ & + \frac{1}{2}\frac{\partial \bar{T}^+}{\partial t}[D-E-F]\frac{1}{1+s\tau_{\mathrm{act}}}\end{aligned} \tag{119}$$

Where:

$$\begin{aligned}A:&\quad \frac{1}{P^+_{\mathrm{H_2,in}}}\frac{\partial P^+_{\mathrm{H_2,in}}}{\partial t} + \left(\frac{-1}{\xi^+_{\mathrm{H_2}}}\frac{\xi^+_{\mathrm{H_2}}}{\partial t}\right) \\ B:&\quad \frac{\tau^{3/2}_{\mathrm{H_2},0}}{2}\left\{\frac{(1-\lambda)\left(\pi_{\mathrm{an}}+P_{\mathrm{O_2,in},0}P^+_{\mathrm{O_2,in}}\right)+\lambda\left(1-P_{\mathrm{O_2,in},0}P^+_{\mathrm{O_2,in}}\right)}{\left(\pi_{\mathrm{an}}+P_{\mathrm{O_2,in},0}P^+_{\mathrm{O_2,in}}\right)P^+_{\mathrm{O_2,in}}}\frac{\partial P^+_{\mathrm{O_2,in}}}{\partial t} + \left(\frac{-1}{\xi^+_{\mathrm{O_2}}}\frac{\partial \xi^+_{\mathrm{O_2}}}{\partial t}\right)\right\}^{-0.5} \\ C:&\quad \frac{1}{P^+_{\mathrm{H_2O,in}}}\frac{\partial P^+_{\mathrm{H_2O,in}}}{\partial t} + \left(\frac{-1}{\xi^+_{\mathrm{H_2O}}}\frac{\partial \xi^+_{\mathrm{H_2O}}}{\partial t}\right) \\ D:&\quad \sinh^{-1}\left(\frac{I}{2I_{\mathrm{ex,ca}}}\right) + \sinh^{-1}\left(\frac{I}{2I_{\mathrm{ex,an}}}\right)\end{aligned} \tag{120}$$

$$E: \quad \frac{I}{4FI_{\text{ex,ca}}^2\sqrt{\left(\frac{I}{2I_{\text{ex,ca}}}\right)^2+1}}\left(\bar{T}_0\bar{T}^+ - 2\Gamma_{\text{ex,ca}}\xi_{\text{ca}}e^{-\frac{\xi_{\text{ca}}}{R\bar{T}}}\right)$$

$$F: \quad \frac{I}{4FI_{\text{ex,an}}^2\sqrt{\left(\frac{I}{2I_{\text{ex,an}}}\right)^2+1}}\left(\bar{T}_0\bar{T}^+ - 2\Gamma_{\text{ex,an}}\xi_{\text{an}}e^{-\frac{\xi_{\text{an}}}{R\bar{T}}}\right)$$

The stack voltage residence time is:

$$\tau_{RS,stack} = \tau_{\text{H}_2} \text{ or } \tau_{\text{O}_2} \text{ or } \tau_{\text{H}_2\text{O}} \tag{121}$$

As shown in Equation (120), the following are the choices available to set the stack voltage residence time: hydrogen pressure inertia first-order delay, oxygen pressure inertia first-order delay, and water pressure inertia first-order delay. The choice will depend on which process is dominant and is system dependent.

The reversible overvoltage characterized time ratio is:

$$\Pi_1 = \frac{FV_0}{\bar{T}_0R} \tag{122}$$

The open-circuit standard condition voltage characterized time ratio is:

$$\Pi_2 = \frac{-49.18-5.44\cdot10^{-3}\cdot\bar{T}_0}{2R} \tag{123}$$

The open-circuit pressure balance voltage characterized time ratio is:

$$\Pi_3 = \ln\left(\frac{\left[\left(\frac{\pi_{\text{ca}}+1}{\pi_{\text{ca}}}\right)^{\lambda}\frac{1}{1+s\tau_{\text{H}_2}}\right]\left[\left(\frac{\pi_{\text{an}}+1}{\pi_{\text{an}}+P_{\text{O}_2,\text{in}}}\right)^{\lambda}\frac{1}{1+s\tau_{\text{O}_2}}\right]}{\left[\left(\frac{\pi_{\text{ca}}-1}{\pi_{\text{ca}}}\right)^{\lambda}\frac{1}{1+s\tau_{\text{H}_2\text{O}}}\right]}\right) \tag{124}$$

The ohmic overvoltage characterized time ratio is:

(125)

The activation overvoltage cathode characterized time ratio is:

$$\Pi_5 = \frac{Z_{\text{ca},0}}{1+s\tau_{\text{act}}}, where\ Z_{\text{ca}}^+ = \frac{Z_{\text{ca}}}{Z_{\text{ca},0}} = \frac{\sinh^{-1}\left(\frac{\frac{\xi_{\text{ca}}}{R\bar{T}}}{\frac{IFe}{R\bar{T}\Gamma_{\text{ex,ca}}}}\right)}{\sinh^{-1}\left(\frac{\frac{\xi_{\text{ca}}}{R\bar{T}_0}}{\frac{IFe}{R\bar{T}_0\Gamma_{\text{ex,ca}}}}\right)} \tag{126}$$

The activation overvoltage anode characterized time ratio is:

$$\Pi_5 = \frac{Z_{\text{an},0}}{1+s\tau_{\text{act}}}, where\ Z_{\text{an}}^+ = \frac{Z_{\text{an}}}{Z_{\text{an},0}} = \frac{\sinh^{-1}\left(\frac{\frac{\xi_{\text{an}}}{R\bar{T}}}{\frac{IFe}{R\bar{T}\Gamma_{\text{ex,an}}}}\right)}{\sinh^{-1}\left(\frac{\frac{\xi_{\text{an}}}{R\bar{T}_0}}{\frac{IFe}{R\bar{T}_0\Gamma_{\text{ex,an}}}}\right)} \tag{127}$$

5.3.3 Thermal Dynamics

The thermal dynamics are divided into two sections: (1) SOEC thermal dynamics and 2) preheater thermal dynamics. Together, both will characterize the full high-temperature hydrogen electrolysis thermal dynamics and will be scaled separately.

5.3.3.1 Solid-Oxide Electrolysis Cell Thermal Dynamics

The following are the relations to normalize each parameter by the selected reference data point:

$$\bar{T}^+ = \frac{\bar{T}}{\bar{T}_0}, \qquad V^+ = \frac{V}{V_0}, \qquad \Delta H^+ = \frac{\Delta H}{\Delta H_0}, \qquad P^+_{\text{heat}} = \frac{P_{\text{heat}}}{P_{\text{heat},0}},$$
$$\theta^+ = \frac{\theta}{\theta_0} = \frac{T_{\text{out}} - T_{\text{in}}}{(T_{\text{out}} - T_{\text{in}})_0}, \qquad P^+_{\text{H}_2,\text{in}} = \frac{P_{\text{H}_2,\text{in}}}{P_{\text{H}_2,\text{in},0}}, \qquad P^+_{\text{H}_2\text{O},\text{in}} = \frac{P_{\text{H}_2\text{O},\text{in}}}{P_{\text{H}_2\text{O},\text{in},0}}, \tag{128}$$
$$P^+_{\text{O}_2,\text{in}} = \frac{P_{\text{O}_2,\text{in}}}{P_{\text{O}_2,\text{in},0}}, \qquad P^+_{\text{N}_2,\text{in}} = \frac{P_{\text{N}_2,\text{in}}}{P_{\text{N}_2,\text{in},0}}$$

From the differential form in Equation (99), normalize and reorganize terms:

$$\begin{aligned}\frac{d\bar{T}^+}{dt} = \quad & \frac{n_c V_0 V^+ I}{\bar{T}_0 c_{\text{P,SOEC}}} - \frac{n_c I \Delta H_0 \Delta H^+_{\text{R}}}{2F\bar{T}_0 c_{\text{P,SOEC}}} + \frac{P_{\text{heat},0} P^+_{\text{heat}}}{\bar{T}_0 c_{\text{P,SOEC}}} \\ & - \frac{\theta_0 \theta^+}{4F\bar{T}_0 c_{\text{P,SOEC}}} \left\{ 2c_{\text{P,H}_2\text{O}} n_c I \pi_{\text{ca}} + \frac{2c_{\text{P,H}_2} n_c I \pi_{\text{ca}} P_{\text{H}_2,\text{in},0} P^+_{\text{H}_2,\text{in}}}{P_{\text{H}_2\text{O},\text{in},0} P^+_{\text{H}_2\text{O},\text{in}}} + c_{\text{P,O}_2} n_c I \pi_{\text{an}} \right. \\ & \left. + \frac{c_{\text{p},N_2} n_c I \pi_{\text{an}} P_{\text{N}_2,\text{in},0} P^+_{\text{N}_2,\text{in}}}{P_{\text{O}_2,\text{in},0} P^+_{\text{O}_2,\text{in}}} \right\}\end{aligned} \tag{129}$$

The SOEC thermal hydraulic residence time is:

$$\tau_{RS,SOEC} = \frac{\bar{T}_0 c_{\text{P,SOEC}}}{P_{\text{heat},0}} \tag{130}$$

The voltage induced power characteristic time ratio is:

$$\Pi_6 = \frac{n_c V_0 I}{P_{\text{heat},0}} \tag{131}$$

The enthalpy change induced power characteristic time ratio is:

$$\Pi_7 = \frac{n_c I \Delta H_0}{2F P_{\text{heat},0}} \tag{132}$$

The cathode water enthalpy change induced power characteristic time ratio is:

$$\Pi_8 = \frac{\theta_0 c_{\text{P,H}_2\text{O}} n_c I \pi_{\text{ca}}}{4F P_{\text{heat},0}} \tag{133}$$

The cathode hydrogen enthalpy change induced power characteristic time ratio is:

$$\Pi_9 = \frac{\theta_0 c_{\text{P,H}_2} n_c I \pi_{\text{ca}} P_{\text{H}_2,\text{in},0}}{4F P_{\text{heat},0} P_{\text{H}_2\text{O},\text{in},0}} \tag{134}$$

The anode oxygen enthalpy change induced power characteristic time ratio is:

$$\Pi_{10} = \frac{\theta_0 c_{\text{P,O}_2} n_c I \pi_{\text{an}}}{4F P_{\text{heat},0}} \tag{135}$$

The anode nitrogen enthalpy change induced power characteristic time ratio is:

$$\Pi_{11} = \frac{\theta_0 c_{\mathrm{P},N_2} n_c I \pi_{\mathrm{an}} P_{\mathrm{N_2,in},0}}{4F P_{\mathrm{heat},0} P_{\mathrm{O_2,in},0}} \tag{136}$$

5.3.3.2 Preheater Thermal Dynamics

The following are the relations to normalize each parameter by the selected reference data point:

$$\begin{aligned} T_{\mathrm{in}}^{+} &= \frac{T_{\mathrm{in}}}{T_{\mathrm{in}}}, \qquad P_{\mathrm{heat,pre}}^{+} = \frac{P_{\mathrm{heat}}}{P_{\mathrm{heat},0}}, \qquad \theta_{\mathrm{steam}}^{+} = \frac{\theta_{\mathrm{steam}}}{\theta_{\mathrm{steam},0}} = \frac{T_{\mathrm{in}} - T_{\mathrm{steam}}}{(T_{\mathrm{in}} - T_{\mathrm{steam}})_0} \\ \theta_{\mathrm{amb}}^{+} &= \frac{\theta_{\mathrm{amb}}}{\theta_{\mathrm{amb},0}} = \frac{T_{\mathrm{in}} - T_{\mathrm{amb}}}{(T_{\mathrm{in}} - T_{\mathrm{amb}})_0}, \qquad P_{\mathrm{H_2,in}}^{+} = \frac{P_{\mathrm{H_2,in}}}{P_{\mathrm{H_2,in},0}}, \qquad P_{\mathrm{H_2O,in}}^{+} = \frac{P_{\mathrm{H_2O,in}}}{P_{\mathrm{H_2O,in},0}}, \\ P_{\mathrm{N_2,in}}^{+} &= \frac{P_{\mathrm{O_2,in}}}{P_{\mathrm{O_2,in},0}}, \qquad P_{\mathrm{N_2,in}}^{+} = \frac{P_{\mathrm{N_2,in}}}{P_{\mathrm{N_2,in},0}} \end{aligned} \tag{137}$$

Non-dimensionalize the inlet temperature from Equation (71) by a certain reference value:

$$\frac{dT_{\mathrm{in}}^{+}}{dt} = \frac{P_{\mathrm{heat,pre}}}{c_{\mathrm{P,pre}} T_{\mathrm{in},0}} - \frac{P_{\mathrm{war,pre}}}{c_{\mathrm{P,pre}} T_{\mathrm{in},0}} + \frac{\epsilon_{\mathrm{rec}} P_{\mathrm{war,pre}}}{c_{\mathrm{P,pre}} T_{\mathrm{in},0}} \tag{138}$$

To consider electrolysis reaction power and steam warming power, plug in Equations (68) and (70):

$$\begin{aligned} \frac{dT_{\mathrm{in}^+}}{dt} = \quad & \frac{P_{\mathrm{heat,pre}}}{c_{\mathrm{P,pre}}} + \frac{(1-\epsilon)}{c_{\mathrm{P,pre}}} \left\{ \theta_{\mathrm{steam}} \left(\frac{c_{\mathrm{P,H_2O}} n_c I \pi_{\mathrm{ca}}}{2F} + \frac{c_{\mathrm{P,H_2}} n_c I \pi_{\mathrm{ca}} P_{\mathrm{H_2,in}}}{2F P_{\mathrm{H_2O,in}}} \right) \right. \\ & \left. - \theta_{\mathrm{amb}} \left(\frac{c_{\mathrm{P,O_2}} n_c I \pi_{\mathrm{an}}}{4F} + \frac{c_{\mathrm{P,N_2}} n_c I \pi_{\mathrm{an}} P_{\mathrm{N_2,in}}}{4F P_{\mathrm{O_2,in}}} \right) \right\} \end{aligned} \tag{139}$$

From Equation (109), non-dimensionalize the preheater thermal dynamics:

$$\begin{aligned} \frac{dT_{\mathrm{in}}^{+}}{dt} = \quad & \frac{P_{\mathrm{heat,pre},0} P_{\mathrm{heat,pre}}^{+}}{c_{\mathrm{P,pre}} T_{\mathrm{in},0}} + \\ & \frac{(1-\epsilon)}{c_{\mathrm{P,pre}} T_{\mathrm{in},0}} \left\{ \theta_{\mathrm{steam},0} \theta_{\mathrm{steam}}^{+} \left(\frac{c_{\mathrm{P,H_2O}} n_c I \pi_{\mathrm{ca}}}{2F} + \frac{c_{\mathrm{P,H_2}} n_c I \pi_{\mathrm{ca}} P_{\mathrm{H_2,in},0} P_{\mathrm{H_2,in}}^{+}}{2F P_{\mathrm{H_2O,in},0} P_{\mathrm{H_2O,in}}^{+}} \right) \right. \\ & \left. - \theta_{\mathrm{amb},0} \theta_{\mathrm{amb}}^{+} \left(\frac{c_{\mathrm{P,O_2}} n_c I \pi_{\mathrm{an}}}{4F} + \frac{c_{\mathrm{P,N_2}} n_c I \pi_{\mathrm{an}} P_{\mathrm{N_2,in},0} P_{\mathrm{N_2,in}}^{+}}{4F P_{\mathrm{O_2,in},0} P_{\mathrm{O_2,in}}^{+}} \right) \right\} \end{aligned} \tag{140}$$

The preheater thermal hydraulic residence time is:

$$\tau_{RS,pre} = \frac{T_{\mathrm{in},0} c_{\mathrm{P,pre}}}{P_{\mathrm{heat,pre},0}} \tag{141}$$

The cathode steam enthalpy change induced power characteristic time ratio is:

$$\Pi_{12} = \frac{(1-\epsilon)\theta_{\mathrm{steam},0} c_{\mathrm{P,H_2O}} n_c I \pi_{\mathrm{ca}}}{F P_{\mathrm{heat,pre},0}} \tag{142}$$

The cathode hydrogen enthalpy change induced power characteristic time ratio is:

$$\Pi_{13} = \frac{(1-\epsilon)\theta_{\mathrm{steam},0} c_{\mathrm{P,H_2}} n_c I \pi_{\mathrm{ca}} P_{\mathrm{H_2,in}}}{F P_{\mathrm{heat,pre},0} P_{\mathrm{H_2O,in}}} \tag{143}$$

The anode oxygen enthalpy change induced power characteristic time ratio is:

$$\Pi_{14} = \frac{(1-\epsilon)\theta_{\mathrm{amb},0} c_{\mathrm{P},\mathrm{O}_2} n_c I \pi_{\mathrm{an}}}{FP_{\mathrm{heat,pre},0}} \tag{144}$$

The anode nitrogen enthalpy change induced power characteristic time ratio is:

$$\Pi_{15} = \frac{(1-\epsilon)\theta_{\mathrm{amb},0} c_{\mathrm{P},\mathrm{N}_2} n_c I \pi_{\mathrm{an}} P_{\mathrm{N}_2,\mathrm{in}}}{FP_{\mathrm{heat,pre},0} P_{\mathrm{O}_2,\mathrm{in}}} \tag{145}$$

5.4 Hydrogen Electrolysis Scaling Summary

The DSS and H2TS scaling were conducted based on a theory developed by Jiangkai [21]. Unfortunately, due to issues with data availability, the data projection could not be demonstrated as was shown for the TEDS case. For the DSS scaling, multiple scaling ratio relations were discovered in Equations (73)–(115) that implicated two or more relations for the same scaling ratio pair. These are products of the law of scaling ratios and can be explained by examining Equation (17). To give an example, presume the effect parameter scaling ratio is about 4 agents of change:

$$\widetilde{\Omega} = X_1\widetilde{\Omega}_1 + X_2\widetilde{\Omega}_2 + X_3\widetilde{\Omega}_3 + X_4\widetilde{\Omega}_4 \tag{146}$$

The effect parameter scaling ratio is:

$$\lambda_A = \frac{\widetilde{\Omega}_M}{\widetilde{\Omega}_P} = \frac{\left(X_1\widetilde{\Omega}_1 + X_2\widetilde{\Omega}_2 + X_3\widetilde{\Omega}_3 + X_4\widetilde{\Omega}_4\right)_M}{\left(X_1\widetilde{\Omega}_1 + X_2\widetilde{\Omega}_2 + X_3\widetilde{\Omega}_3 + X_4\widetilde{\Omega}_4\right)_P} \tag{147}$$

Although there may be numerous combinations to satisfy the designated λ_A given the variation of effect parameter values, the simplest and strictest method is to enforce each individual effect parameter scaling ratio to be the global value:

$$\lambda_A = \frac{X_{M,1}\widetilde{\Omega}_{M,1}}{X_{P,1}\widetilde{\Omega}_{P,1}} = \frac{X_{M,2}\widetilde{\Omega}_{M,2}}{X_{P,2}\widetilde{\Omega}_{P,2}} = \frac{X_{M,3}\widetilde{\Omega}_{M,3}}{X_{P,3}\widetilde{\Omega}_{P,3}} = \frac{X_{M,4}\widetilde{\Omega}_{M,4}}{X_{P,4}\widetilde{\Omega}_{P,4}} \tag{148}$$

If applied, it is clear more than one relation can be determined. If ω-strain or identity coordinate transformation is not applied, then λ_A value is possibly not predetermined. If this is the case, more than one λ_A value exists depending on how the nominal values are chosen. It would be depend on any user or project objectives whether or not to preserve the parameter of interest dynamically.

Identically, more than expression for stack voltage $\left(\lambda_{A,V}\right)$, differential stack voltage $\left(\lambda_{B,V}\right)$, differential average stack temperature $\left(\lambda_{B,\bar{T}}\right)$, and differential inlet temperature $\left(\lambda_{B,T_{\mathrm{in}}}\right)$ have been derived with separate terms, allowing degrees of freedom to scale the SOEC system. One good aspect of having multiple possible expressions is that it connects one phenomenon to another. For example, if the cathode inlet-steam temperature difference with water-specific heat determined the differential inlet temperature scaling ratio $\left(\lambda_{B,T_{\mathrm{in}}}\right)$ as shown in Equation (112), other undetermined terms in Equation (113) can be calculated. Once data are acquired, a demonstration of the developed theory will be conducted.

For the H2TS, all residence times and characterized time ratios were derived and are ready for data input. Depending on the system operations, it may be possible to satisfy all target residence times and have near similarity for characterized time ratio values at the same time. If coupled fluid properties such as temperature and specific heat are as restrictive as experienced with the TEDS case, it is predicted that some conditions will have to be ignored to proceed.

6. DATA PROJECTION ERROR DETERMINATION

One role of the projected data is to determine the valid range of values for each time step. Since the data projection is based on previously generated data, it is anticipated that the error from experimental measurements may propagate to the projected data. To explore this, the error propagation analysis has been conducted for DSS from value normalization to separation calculation. The simplest form of error propagation [23] can be expressed as the following:

$$\text{For } u(x,y,\dots) \rightarrow \sigma_u^2 = \left(\frac{\partial u}{\partial x}\right)^2 \sigma_x^2 + \left(\frac{\partial u}{\partial y}\right) \sigma_y^2 + \cdots \tag{149}$$

Where function u is about x, y, and other arbitrary parameters. The error propagation from normalization is the following:

$$\beta = \frac{u}{u_0} \rightarrow \sigma_\beta = \sqrt{\left(\frac{\partial \beta}{\partial u}\right)^2 \sigma_u^2 + \left(\frac{\partial \beta}{\partial u_0}\right)^2 \sigma_{u_0}^2} = \frac{\sigma_u}{u_0} \tag{150}$$

The agents of change can be described as a second order central first derivative of the parameter of interest:

$$\omega = \frac{d\beta}{dt} \approx \frac{\beta_{i+1} - \beta_{i-1}}{\Delta t} \tag{151}$$

The agent of change error propagation is:

$$\begin{aligned} \omega \approx \frac{\beta_{i+1} - \beta_{i-1}}{\Delta t} \rightarrow \sigma_\omega = & \sqrt{\left(\frac{\partial \omega}{\partial \beta_{i+1}}\right)^2 \sigma_{\beta_{i+1}}^2 + \left(\frac{\partial \omega}{\partial \beta_{i-1}}\right)^2 \sigma_{\beta_{i-1}}^2} \\ = & \sqrt{\frac{\sigma_{\beta_{i+1}}^2 + \sigma_{\beta_{i-1}}^2}{\Delta t^2}} \end{aligned} \tag{152}$$

The error propagation of the agent of change first derivative is identical to the agent of change:

$$\begin{aligned} \omega' \approx \frac{\beta_{i+1} - 2\beta_i - \beta_{i-1}}{\Delta t^2} \rightarrow \sigma_{\omega'} = & \sqrt{\left(\frac{\partial \omega'}{\partial \beta_{i+1}}\right)^2 \sigma_{\beta_{i+1}}^2 + \left(\frac{\partial \omega'}{\partial \beta_i}\right)^2 \sigma_{\beta_i}^2 + \left(\frac{\partial \omega'}{\partial \beta_{i-1}}\right)^2 \sigma_{\beta_{i-1}}^2} \\ = & \sqrt{\frac{\sigma_{\beta_i+1}^2 + \sigma_{\beta_i}^2 + \sigma_{\beta_{i-1}}^2}{\Delta t^4}} \end{aligned} \tag{153}$$

The error propagation of the process time is:

$$\tau = \frac{\beta}{\omega} \rightarrow \sigma_\tau = \sqrt{\left(\frac{\partial \tau}{\partial \beta}\right)^2 \sigma_\beta^2 + \left(\frac{\partial \tau}{\partial \omega}\right)^2 \sigma_\omega^2} = \sqrt{\left(\frac{1}{\omega}\frac{\partial \tau}{\partial t}\right)^2 \sigma_\beta^2 + \left(\frac{1}{\omega'}\frac{\partial \tau}{\partial t}\right)^2 \sigma_\omega^2} \tag{154}$$

The temporal displacement rate first derivative is:

$$\frac{dD}{dt} = \frac{-1}{\omega}\frac{d\omega}{dt} + \frac{2\beta}{\omega^3}\frac{d\omega}{dt} - \frac{\beta}{\omega}\frac{d^2\omega}{dt^2} \tag{155}$$

The error propagation of the temporal displacement rate:

$$D = -\frac{\beta}{\omega^2}\frac{d\omega}{dt} \rightarrow \sigma_D = \sqrt{\left(\frac{\partial D}{\partial \beta}\right)^2 \sigma_\beta^2 + \left(\frac{\partial D}{\partial \omega}\right)^2 \sigma_\omega^2 + \left(\frac{\partial D}{\partial \omega'}\right)^2 \sigma_{\omega'}^2}$$
$$= \sqrt{\left(\frac{1}{\omega}\frac{\partial D}{\partial t}\right)^2 \sigma_\beta^2 + \left(\frac{1}{\omega'}\frac{\partial D}{\partial t}\right)^2 \sigma_\omega^2 + \left(\frac{1}{\omega''}\frac{\partial D}{\partial t}\right)^2 \sigma_{\omega'}^2} \quad (156)$$

The process action can be expressed in terms of the trapezoidal numerical integration:

$$\tau_S = \int (1 + D)\, dt = \sum_{k=1}^{N} \left[\frac{(1+D)_{k-1} + (1+D)_k}{2} \Delta x_k\right] \quad (157)$$

The error propagation of the trapezoidal numerical integration error propagation is:

$$\sigma_{\tau_S} = \sqrt{\left(\frac{\Delta x_0}{2}\right)^2 \sigma_{(1+D)_0}^2 + \sum_{k=1}^{N-1}[(\Delta x_1 + \Delta x_{k+1})^2 \sigma_k^2] + \left(\frac{\Delta x_N}{2}\right)^2 \sigma_{(1+D)_N}^2} \quad (158)$$

Before proceeding to other terms, the process action is a scalar that represents the process time elapsed. The derivative of a scalar is 0:

$$\frac{d\tau_S}{dt} = 0 \quad (159)$$

Now, consider the error propagation of the effect parameter (normalized agent of change):

$$\widetilde{\Omega} = \tau_S \omega \rightarrow \sigma_{\widetilde{\Omega}} = \sqrt{\left(\frac{\partial \widetilde{\Omega}}{\partial \tau_S}\right)^2 \sigma_{\tau_S}^2 + \left(\frac{\partial \widetilde{\Omega}}{\partial \omega}\right)^2 \sigma_\omega^2} \quad (160)$$

The derivative is a term to track changes upon a certain measured length or duration. Since the process action is a scalar, the error propagation contribution from the process action is negligible:

$$\sigma_{\widetilde{\Omega}} = \tau_S \sigma_\omega \quad (161)$$

The error propagation of the normalized process time is:

$$\tilde{\tau} = \frac{\tau}{\tau_S} \rightarrow \sigma_{\tilde{\tau}} = \sqrt{\left(\frac{\partial \tilde{\tau}}{\partial \tau_S}\right)^2 \sigma_{\tau_S}^2 + \left(\frac{\partial \tilde{\tau}}{\partial \tau}\right)^2 \sigma_\tau^2} = \frac{\sigma_\tau}{\tau_S} \quad (162)$$

The projected data are:

$$\lambda_A = \frac{\widetilde{\Omega}_M}{\widetilde{\Omega}_P} \rightarrow \widetilde{\Omega}_M = \lambda_A \widetilde{\Omega}_P \quad (163)$$

The error propagation of the projected data is:

$$\sigma_M = \sqrt{\left(\frac{\partial \widetilde{\Omega}_M}{\partial \lambda_A}\right)^2 \sigma_{\lambda_A}^2 + \left(\frac{\partial \widetilde{\Omega}_M}{\partial \widetilde{\Omega}_P}\right)^2 \sigma_{\widetilde{\Omega}_P}^2} \quad (164)$$

The parameter of interest scaling ratio is a scalar, thus:

$$\sigma_M = \lambda_A \sigma_{\widetilde{\Omega}_P} \quad (165)$$

The error propagation of the measured separation is in Equation (165) and is illustrated in Figure 29. In that account, the existing errors in the base are propagated to the projected data and it is recommended to determine the value. The user should consider that for the chosen confidence, the experimental or simulated case of the propagated system should be within the error band provided all dominant physics are included in the scaling analysis. If there are transients that exhibit disagreeing behavior, the issue is not the projected case experiment data or simulation data failing to fit within the error bar but is possibly caused by the lack of known physics, inappropriate assumptions, or using incorrect models.

$$\begin{aligned}\sigma_\eta = & \sqrt{\left(\frac{\partial\eta}{\partial\beta_P}\right)^2\sigma_{\beta_P}^2+\left(\frac{\partial\eta}{\partial D_P}\right)^2\sigma_{D_P}^2+\left(\frac{\partial\eta}{\partial\widetilde{\Omega}_P}\right)^2\sigma_{\widetilde{\Omega}_P}^2+\left(\frac{\partial\eta}{\partial\widetilde{\Omega}_M}\right)^2\sigma_{\widetilde{\Omega}_M}^2} \\ = & \left(\frac{\partial\eta}{\partial t_P}\frac{\partial t_P}{\partial\beta_P}\right)^2\sigma_{\beta_P}^2+\left(\frac{\partial\eta}{\partial t_P}\frac{\partial t_P}{\partial D_P}\right)^2\sigma_{D_P}^2+\left(\frac{\partial\eta}{\partial t_P}\frac{\partial t_P}{\partial\widetilde{\Omega}_P}\right)^2\sigma_{\widetilde{\Omega}_P}^2+\left(\frac{\partial\eta}{\partial t_M}\frac{\partial t_M}{\partial\widetilde{\Omega}_M}\right)^2\sigma_{\widetilde{\Omega}_M}^2\end{aligned} \tag{166}$$

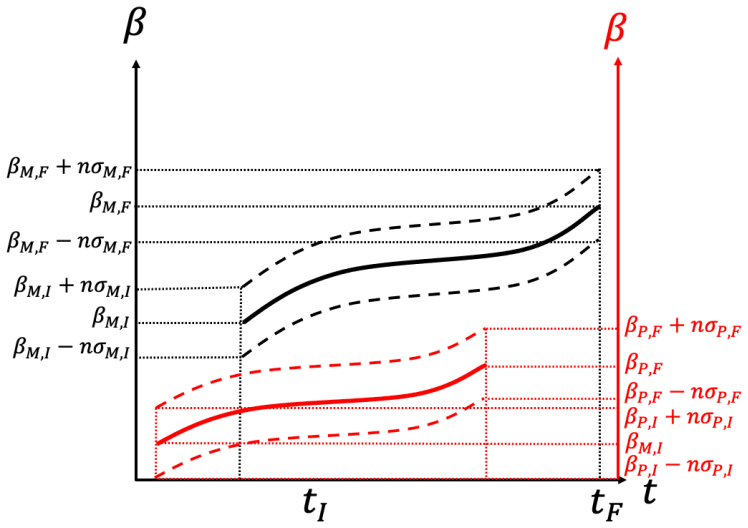

Figure 29. Base (β_P) and projected (β_M) data with random error variations.

The net standard error can be defined as the combined random systematic error [23]:

$$\sigma_{net}=\sqrt{\sigma_{random}^2+\sigma_{systematic}^2} \tag{167}$$

While random errors are unavoidable, fluctuations or noise of measurement method may underpredict or overpredict at any given time, while systematic errors are consistent behaviors that can be replicated by experiment repetition. The error propagation analysis conducted for DSS is the assessment that quantifies the amount error inherited from base data. Unless otherwise reported, the determined error propagation is a form of random error estimation in separation measurements:

$$\sigma_{random}=\sigma_\eta \tag{168}$$

Therefore, the projected data can be plotted with error bands for the chosen grade of confidence. Interestingly, by assessing the full transient data via DSS, the standard error in respect to the transient behavior is determined:

$$\eta_k = \beta_{P,k}\sqrt{\varepsilon D_{P,k}}\left(\frac{1}{\widetilde{\Omega}_{P,k}} - \frac{1}{\widetilde{\Omega}_{M,k}}\right) \tag{169}$$

$$\sigma_{DSS} = \sqrt{\frac{1}{N}\sum_{k=1}^{N}\eta_k^2} \tag{170}$$

Where η_k is the measured local separation for every time stamp at k $(k = 1, \dots, N)$ and σ is the standard error considering each local separation as the deviation from ideal values. For a given experiment, it is expected that the repetition of the same operational procedures would yield the same results. Thus, the measured standard error via DSS for a data set in comparison to some ideal or desired data set will remain constant unless settings are modified. The consistent behavior of the DSS measured standard error suggests it is a form of systematic error:

$$\sigma_{systematic} = \sigma_{DSS} \tag{171}$$

The net error of the measured separation is:

$$\sigma_{net} = \sqrt{\sigma_\eta^2 + \sigma_{DSS}^2} \tag{172}$$

The net error derived is defined in the β-$\widetilde{\Omega}$ phase space and is helpful for determining and visualizing the valid range. For users, the phase-space representation may be less useful due to the unique coordinate system and difficult to associate the raw and postprocessed data. To provide a more helpful data representation, the determined transient standard error can be reorganized in terms of the raw form data. First, assume the net error is known, calculated by. Equation (171). Then, the margin of error for the given confidence is:

$$Band = \pm z^* \frac{\sigma_{net}}{\sqrt{N}} \tag{173}$$

Where z^* is the level of confidence. The confidence interval of the separation is:

$$\beta_{P,k}\sqrt{\varepsilon D_{P,k}}\left(\frac{1}{\widetilde{\Omega}_{P,k}} - \frac{1}{\widetilde{\Omega}_{M,k}}\right) = \pm z^* \frac{\sigma_{net}}{\sqrt{N}} \tag{174}$$

By reorganizing Equation (173), the possible lower and upper bound values of the projected effect parameter if the given margin of errors are true is:

$$\widetilde{\Omega}_M = \frac{\beta_P \widetilde{\Omega}_P \sqrt{\varepsilon D_P}}{\beta_P \sqrt{\varepsilon D_P} \mp \widetilde{\Omega}_P z^* \frac{\sigma_{net}}{\sqrt{N}}} \tag{175}$$

When DSS scaling activitiy is concluded, the time ratio is either predetermined or derived. Using Equation (14), the projected process action is:

$$\tau_{M,S} = \tau_{P,S} t_R \tag{176}$$

Using the projected process action from Equation (175) and the relation in Equation (8), the projected agent of change is:

$$\omega_M = \frac{\widetilde{\Omega}_M}{\tau_{M,S}} \tag{177}$$

Similarly, the projection process time can be determined from Equation (14):

$$\tau_M = \tau_P t_R \tag{178}$$

From Equation (5), the projected parameter of interest is:

$$\beta_M = \omega_M \tau_M = \frac{\tilde{\tau}\beta_P \tilde{\Omega}_P \sqrt{\varepsilon D_P}}{\beta_P \sqrt{\varepsilon D_P} \mp \tilde{\Omega}_P z^* \frac{\sigma_{net}}{\sqrt{N}}} \tag{179}$$

Given the projected parameter of interest, the projected confidence interval is:

$$\beta_{pro} = \beta_M + \frac{\tilde{\tau}\beta_P \tilde{\Omega}_P \sqrt{\varepsilon D_P}}{\beta_P \sqrt{\varepsilon D_P} \mp \tilde{\Omega}_P z^* \frac{\sigma_{net}}{\sqrt{N}}} \tag{180}$$

The distribution of the projected data is user and system dependent.

7. FUTURE WORK

The next steps going into FY2023 is to develop a three-part workflow in preparation for mock user case demonstrations. First, scaling of other DETAIL facilities is required. To prepare for a fully functioning IES network emulation, scaling will aid researchers in determining how signals should be reconfigured. Second, similar to the data generation for the TTSS shown in Section 4.2, all systems should project data and conduct the proposed experiment either physically or via simulation to validate the developed theory. Last is the design and commencement of the full IES DETAIL network. The steps laid out below are required before proceeding to user case scenarios.

This will be accomplished after the work is completed in FY2022. Although the partial scaling of DETAIL facilities has been conducted for TEDS and HTHE, the scaling analyses of the coupled piping and heat exchangers (HX) are necessary as well. When physically connected, the shared components (i.e., the HX for TEDS and HTHE) can be scaled on either end to act as the common denominator to associate scaling ratios or characterized time ratios of one system to another. This would enable synchronized transient interactions, which are virtually connected systems with sections that represent quantity in/out, which will be scaled.

Once accomplished, the scaling and testing phases for the individual DETAIL facility scaling will begin. The main motivation is to ensure the data projections are accurate enough for the cross-system interactions phase. The demonstrated projections based on previous data alone do not prove the newly calculated data to be true. There are cases where the modeled governing equations lack essential physics to correctly capture the evolving phenomena or inappropriate assumptions that may have led to discrepancies. To complete this task, two elements are required: the individual design and data of a consistent experiment for each DETAIL facility and running the projected experiment design to measure the scaling distortion. Other than TEDS and HTHE, coordination with the Microreactor Agile Non-Nuclear Experimental Testbed (MAGNET) facility has been initiated and RELAP5-3D model development is planned for next fiscal year to determine governing equations.

The design to create a DETAIL universal experiment will be pivotal to the success of demonstrating the IES network emulation on the engineering scale. Communication on all sides is essential and any facility changes will have to be conveyed promptly for scaling ratio-related adjustments. Although it is undetermined on how to have systems work jointly from a technical standpoint, INL-developed tools such as Deep-Lynx or future proposed IES work for real-time optimization are feasible options. However, because data management tool development is currently outside the scope of this project, this should be solved by the responsible research group. To test DETAIL network coordination with external facilities, the MAGNET and Microreactor Applications Research Validation and Evaluation (MARVEL) projects are an excellent pair as both are microreactor-related experimental facilities. As a preliminary study, scaling of MARVEL will be considered and efforts to comprehend facility functions using open-source information are pending future work.

One potential development is the research of structuring DSS code validation and verification (V&V) and uncertainty quantification (UQ). Using the unique metrics provided by DSS, when and how much

distortion can be measured for given systems can be detected. The metric should be capable of conducting sensitivity analyses for various forms of perturbations applied to simulations and confirm applicable input ranges for the code models. The proposed development will have to derive a DSS-specific acceptance criteria based on statistics and/or differential geometry to determine the threshold of measured distortion and uncertainty. Coupled with the Department of Energy's INL-led IES program, this new capability could be another service provided to future users.

8. CONCLUSION

The TTSS of TEDS and SOEC of HTHE were selected to represent cases of data extrapolation to design facility tests based on the generated data. Based on flow conditions, geometry, materials, and transient behavior, the fundamental equations were determined to include TTSS and SOEC fluid, thermal, and unique physic parameters (porosity for TTSS and Gibbs free energy for SOEC). The equations were non-dimensionalized according to the DSS and H2TS definitions, and scaled formats were derived for the relevant phase-space coordination transformation methods (DSS). Characterized time ratios (H2TS) were introduced in Table 1 and Equation (23). For the demonstration using past data, TTSS accelerated data projection was the only case conducted due to limitations in acquiring SOEC experimental data.

To accelerate the given TTSS data in the DSS definition, static time-scaling methods, such as dilation and identity, were excluded from the analysis. By setting the TTSS centerline mid-axial temperature as the property to preserve, the phase-space scaling was further restricted to the ω-strain method (i.e., the normalized temperature scaling ratio was $\lambda_A = 1$). This was done to maintain identical relative TTSS temperature magnitudes when normalizing with the temperature recorded during the transition between charging and discharging transients. To be capable of $\lambda_A \neq 1$, the value used to normalize the TTSS temperature either must be derived or be a constant that is shared between the original and accelerated test cases. When attempting to make λ_A equivalent to the time ratio (β-strain scaling method), it was concluded that the goal time ratio could not be achieved due to the balance of the therminol fluid density, therminol fluid specific heat, and the stainless-steel wall conductive heat transfer coefficient when the TTSS fluid temperature was altered. For H2TS, the stored heat was preserved by ensuring the energy residence time is half and each energy characteristic time is near prototypic values.

After setting the global time ratio to 0.5 (twice as fast) and following the ω-strain scaling for DSS and typical scaling for H2TS, the scaling ratios for the TTSS inlet, outlet, and wall parameters were calculated and are shown in Table 3 and Table 5. As anticipated, the derived DSS twice-accelerated case showed perfect scaling for the TTSS temperature β-$\widetilde{\Omega}$ distributions (overlapping of data is proof of ideal scaling) and demonstrated the data drift in comparison to the original data set using β–time representation. On the other hand, the other scaled parameters showed shifts toward the β-$\widetilde{\Omega}$ distribution as well; however, when dividing the scaling ratios into the corresponding parameters, the accelerated data overlapped to indicate perfect scaling. The data extrapolation was successful and provided a TTSS test that achieved the same energy charge and discharge in half the time. For the derived H2TS twice-accelerated case, although the momentum residence time could not be half at the same chosen nominal time as the energy residence time, the energy scaling distortion was minimized by parametrically determining the near-ideal conditions to match prototypic characteristic momentum and energy time ratios as shown in Table 5. The momentum residence time ratio suggests the momentum-related phenomena to be more than 6 times accelerated. Considering flow conditions in the TTSS with porosity of 0.6, possible transitions to different flow regimes may occur more prominently than the DSS momentum scaled equations.

While abiding by scaling restrictions, such as unchanged geometry and materials, the accelerated test was calculated by extrapolating the original data set using the DSS and H2TS methodology. One of the unexpected yet significant findings of this scaling activity was that without the freedom to change the geometry of the system, the scaling ratios were about system properties (e.g., fluid density). The distribution of these properties varied from one to another and restricted the range of feasible scaling ratio values. For future reference, if more dramatic test acceleration without varying geometry were desired, a change in the fluid medium of the TTSS would have to be considered.

Similar scaling was done for the HTHE facility using the same procedures shown in Section 4. As noted in Section 5.4, all DSS scaling ratios and H2TS characteristic time ratios were derived without base data to project. Until further coordination with the HTHE group, this effort will be delayed to FY2023.

To explore error propagations in the projected data, the theory outlook was conducted, and new content was discovered for DSS-related standard errors. The distinction between random and systematic errors were considered, which led to the conclusion that DSS's calculated transient standard error is systematic and errors propagated from the measured data are random. For future work, the net error will be used as the standard method to evaluate the similarity data geometry and determine the confidence interval of the projected data.

9. REFERENCES

[1] Morton, Terry James. 2020. "Integrated Energy Systems Experimental Systems Development". United States. https://www.osti.gov/servlets/purl/1668842.

[2] Al-Ghussain, Loiy; Abubaker, Ahmad M., Darwish Ahmad, Adnan. 2021. "Superposition of Renewable-Energy Supply from Multiple Sites Maximizes Demand-Matching: Towards 100% Renewable Grids in 2050." *Appl. Energy 284*, 116402. https://doi.org/10.1016/j.apenergy.2020.116402.

[3] Levin, Todd, Botterud, Audun, Mann, W. Neal, Kwon, Jongwan, Zhou, Zhi. 2022. "Extreme Weather and Electricity Markets: Key Lessons from the February 2021 Texas Crisis." *Joule* 6, 1–7. https://doi.org/10.1016/j.joule.2021.12.015.

[4] Eliana, R. 2022. "Argentina Capital Hit by Major Power Outage Amid Heat Wave." News Article: Reuters. 11 January 2022. Available online: https://www.reuters.com/world/americas/argentina-capital-hit-by-major-power-outage-amid-heat-wave-2022-01-11/.

[5] Asgary, Ali and Mousavi-Jahromi, Yeganeh. 201. "Power Outage, Business Continuity and Businesses' Choices of Power Outage Mitigation Measures." *American Journal of Economics and Business Administration* 3. 312-320. https://doi.org/10.3844/ajebasp.2011.307.315.

[6] Bragg-Sitton, Shannon M. 2022. "Next Generation Nuclear Energy: Advanced Reactors and Integrated Energy Systems". United States. https://www.osti.gov/servlets/purl/1865609.

[7] Marting, Robert P. and Frepoli, Cesare, *Design-Basis Accident Analysis Methods for Light-Water Nuclear Power Plants*, World Scientific: Singapore, 2019, 181–263. https://doi.org/10.1142/11139.

[8] Xiangbin, Li, Nan, Li, Wu, Qiao, Zhang, Hengyu, Muhammad, Abdus Samad, Lu, Daogang. 2019. "Application of dynamical system scaling method on simple gravity-driven draining process." *Journal of Nuclear Science and Technology* 55, 11-18. https://doi.org/10.1080/00223131.2017.1372231.

[9] Yoshiura, Ramon Ken, Epiney, Aaron S, and M Mostafa Abdo, Mohammad Gamal. 2021. "Integration of Dynamical System Scaling to RAVEN and Facility Application". United States. https://www.osti.gov/servlets/purl/1822257.

[10] Yoshiura, R.K. "Dynamic System Scaling Application to Accelerated Nuclear Fuel Testing." *In Proceedings of the 19th International Topical Meeting on Nuclear Thermal Hydraulics*, Brussels, Belgium, 6–11 March 2022.

[11] Sabharwall, Piyush, O'Brien, James E., McKellar, Michael G., Housley, Gregory K., and Bragg-Sitton, Shannon M. 2015. "Scaling Analysis Techniques to Establish Experimental Infrastructure for Component, Subsystem, and Integrated System Testing". United States. https://doi.org/10.2172/1186749.

[12] Frick, Konor, Bragg-Sitton, Shannon, and Rabiti, Cristian. 2020. "Modeling the Idaho National Laboratory Thermal-Energy Distribution System (TEDS) in the Modelica Ecosystem" *Energies* 13, no. 23: 6353. https://doi.org/10.3390/en13236353.

[13] Stoots, Carl M., Duenas, Alexander, Sabharwall, Piyush, O'Brien, James E., Yoo, Jun Soo, and Bragg-Sitton, Shannon M. 2018. "Thermal Energy Delivery System Design Basis Report". United States. https://doi.org/10.2172/1756571.

[14] Frick, Konor L, Bragg-Sitton, Shannon M, and Garrouste, Marisol. 2021. "Validation and Verification for INL Modelica-based TEDS models Via Experimental Results". United States. https://doi.org/10.2172/1836100.

[15] Reyes, Jose. 2015. "The Dynamical System Scaling Methodology." *In Proceedings of the 16th International Topical Meeting on Nuclear Thermal Hydraulics*, Chicago, IL, USA, 30 August–4 September 2015.

[16] Reyes, Jose N., Frepoli, Cesare, and Yurko, Joseph. 2015. "The Dynamical System Scaling Methodology: Comparing Dimensionless Governing Equations with the H2TS and FSA Methodologies." *In Proceedings of the 16th International Topical Meeting on Nuclear Thermal Hydraulics*, Chicago, IL, USA, 30 August–4 September 2015.

[17] Brown, G. Burniston. 1939. "The Evolution of Physics: The Growth of Ideas from the Early Concepts to Relativity and Quanta. By Albert Einstein and Leopold Infeld. (Cambridge: at the University Press, 1938. Pp. x 319. Price 8s. 6d.)." *Philosophy* 14 (54). Cambridge University Press: 242–42. https://doi.org/10.1017/S0031819100011670.

[18] D.J Gunn. 1978. "Transfer of heat or mass to particles in fixed and fluidised beds" *Int. J. Heat Transf. 21*, 467. https://doi.org/10.1016/0017-9310(78)90080-7.

[19] Esence, Thibaut, Bruch, Arnaud, Molina, Sophie, Stutz, Benoit, and Fourmigué, Jean-François. 2017. "A review on experience feedback and numerical modeling of packed-bed thermal energy storage systems" *Solar Energy* 153, 628-654. https://doi.org/10.1016/j.solener.2017.03.032.

[20] Yoshiura, Ramon, Duenas, Alexander, and Epiney, Aaron. 2022. "Dynamical System Scaling of a Thermocline Thermal Storage System in the Thermal Energy Distribution System (TEDS) Facility" *Energies* 15, no. 12: 4265. https://doi.org/10.3390/en15124265.

[21] Peng, Jiangkai, and Westover, Tyler. "Solid Oxide Electrolysis Cell System Dynamic Model" Unpublished manuscript, September 14 2021, typescript.

[22] Stoots, Carl, and O'Brien, James. 2018. "Nuclear Science and Technology: High Temperature Electrolysis". United States.

[23] Kirkup, Les, and Frenkel, R.B. 2006. "Systematic Errors." Chapter. In *An Introduction to Uncertainty in Measurement: Using the GUM (Guide to the Expression of Uncertainty in Measurement)*, 83–96. Cambridge: Cambridge University Press. https://doi.org/10.1017/CBO9780511755538.008.